Title
High-Throughput In Situ Parametric Studies of Cytochrome P450 Catalysis

Author
Traylor, Matthew John

Publication Date
2010

Peer reviewed|Thesis/dissertation

High-Throughput *In Situ* Parametric Studies of Cytochrome P450 Catalysis

By

Matthew John Traylor

A dissertation submitted in partial satisfaction of the

requirements for the degree of

Doctor of Philosophy

in

Chemical Engineering

in the

Graduate Division

of the

University of California, Berkeley

Committee in charge:

Professor Douglas S. Clark, Chair
Professor Harvey Blanch
Professor Chris Chang
Professor Jonathan Dordick

Fall 2010

High-Throughput *In Situ* Parametric Studies of Cytochrome P450 Catalysis

by

Matthew John Traylor

Abstract

High-Throughput *In Situ* Parametric Studies of Cytochrome P450 Catalysis

by

Matthew John Traylor

Doctor of Philosophy in Chemical Engineering
University of California, Berkeley
Professor Douglas S. Clark, Chair

Cytochrome P450 enzymes are the main route of first pass oxidative metabolism of prescribed drugs in humans. As such, they are of paramount importance to the pharmaceutical industry in the metabolic and toxicity screening of lead compounds. P450 enzymes function by generating a highly reactive ferryl-oxo species with two electrons supplied via NADPH. This reactive species is capable of a wide range of oxidative transformations, often on unreactive carbon centers. Consequently, P450 enzymes are of general interest to the biotechnology industry due to the variety of enantioselective oxidation reactions that they catalyze.

The effective utilization of P450 enzymes within both industries has yet to be realized. In the biotech industry, P450 transformations have not been adopted, except in whole cell systems, due to slow reaction rates and an inefficient use of the expensive cofactor, NADPH. The P450 reaction mechanism often yields a broad array of coupled and uncoupled products from a single substrate. While it is well known that reaction conditions can drastically affect the rate of P450 catalysis, their effects on regioselectivity and coupling are not well characterized. To investigate such effects, the CYP1A2 oxidation of 7-ethoxymethoxy-3-cyanocoumarin (EOMCC) was examined as a function of buffer type, buffer concentration, pH, and temperature. A high-throughput, optical method was developed to simultaneously measure the rate of substrate depletion, NADPH depletion, and generation of the O-dealkylated product. Increasing the phosphate buffer concentration and temperature increased both the NADPH and EOMCC depletion rates by 6-fold, whereas coupling was constant at 7.9% and the regioselectivity of O-dealkylation to other coupled pathways was constant at 21.7%. Varying the buffer type and pH increased NADPH depletion by 2.5-fold and EOMCC depletion by 3.5-fold; however, neither coupling nor regioselectivity was constant, with variations of 14.4% and 21.6%, respectively. Because the enzyme-substrate binding interaction is a primary determinant of both coupling and regioselectivity, it is reasonable to conclude that ionic strength, as varied by the buffer concentration, and temperature alter the rate without affecting binding while buffer type and pH alter both.

Although the large effect of ion type and concentration on cytochrome P450 catalysis is well documented, the full kinetic consequence of this effect has yet to be explored. We measured the CYP1A2 and CYP3A4 mediated O-dealkylation of alkoxycoumarins as a function of ion type and concentration for twelve salts. We found that greatest rate enhancement for both isoforms with potassium fluoride, yielding increases of 19 and 2.5 fold for CYP3A4 and CYP1A2, respectively. Moreover, we

measured the kinetic parameters and noncompetitive intermolecular isotope effect for the O-dealkylation of 7-methoxy-3-cyanocoumarin by CYP1A2 as a function of potassium fluoride and P450-reductase content. We found the rate increases seen with potassium fluoride were primarily due to increases in k_{cat}. Furthermore, the noncompetitive intermolecular isotope effect was large (~6) and constant for all conditions assayed. A simplified P450 mechanism was used to support the possibility that the large isotope effects seen in this and other P450 systems are due primarily to the large rate of uncoupling, which serves to unmask the intrinsic isotope effect.

In vitro metabolic stability measurements are a critical component of pre-clinical drug development in the pharmaceutical industry. Available measurement strategies rely on chromatography and mass spectrometry, which are expensive, labor-intensive, and low-throughput. Using a reaction engineering approach, we have developed a general method to measure metabolic stability by fluorescently quantifying cofactors in the mechanisms of cytochrome P450 enzymes. This method combines the accuracy and generality of chromatography with the ease and throughput of fluorescence.

To my family

Table of Contents

Acknowledgements

I would like to acknowledge the important contribution of the undergraduate researchers that helped me complete this thesis. Jack Chai, Eric Arnon, Larry Gao, and Michael Lin all brought an impressive dedication and good spirit to our work. Their contributions were limited only by my ability to advise them.

I would also like to acknowledge the helpful presence of my advisor, Doug Clark. The space that he gave me during graduate school taught me to be an independent and proactive researcher. Finally, I appreciate that he approaches his students as people and not as equipment.

I must also acknowledge the contributions of my lab mates, who have been excellent examples for me, both personally and professionally. Group meetings in the Clark Lab offered a weekly reconnection with the benefits of vigorous debate and strict peer review, which has shaped the way that I interact with scientists and research in general.

Finally, the contribution of other friends, colleagues, and roommates has been invaluable in my experience of graduate school.

CHAPTER 1

Introduction

1.1 Overview

Cytochrome P450 enzymes comprise a superfamily of heme-thiolate monooxygenases present in all types of life that catalyze a diverse array of biological transformations (1). The full P450 reaction mechanism is shown in Figure 1.1. In this general scheme, the P450 enzyme functions as a monooxygenase, wherein one atom of oxygen from dissolved dioxygen is incorporated into the substrate and the other produces water. The P450 active site is focused at the iron center of a heme cofactor, which is anchored to the protein via a cysteine residue. Two electrons are sequentially shuttled to the enzyme to activate dioxygen in a series of steps culminating in the generation of a highly reactive iron-oxo species that is responsible for substrate oxidation (*2*).

The prototypical P450 reaction is the addition of a hydroxyl group at a non-activated carbon center; however, many other mechanisms are possible (*3*). In addition to the oxidation of substrate, there are several branch points leading to uncoupling pathways, where the supply of reducing equivalents to the P450 is not coupled to product generation. The autooxidation shunt occurs when superoxide dissociates from the ferric-superoxo intermediate formed after the first 1-electron reduction. Following the second 1-electron reduction, peroxide species can also dissociate. This is believed to occur when excess water in the active site disrupts the series of proton transfer events necessary to transition from the ferric-peroxo intermediate to the active iron-oxo species (*4*). These uncoupling pathways drain electrons from the system, decreasing the overall reaction efficiency and rate of product formation. In addition, the reactive oxygen species formed can lead to protein deactivation (*5*).

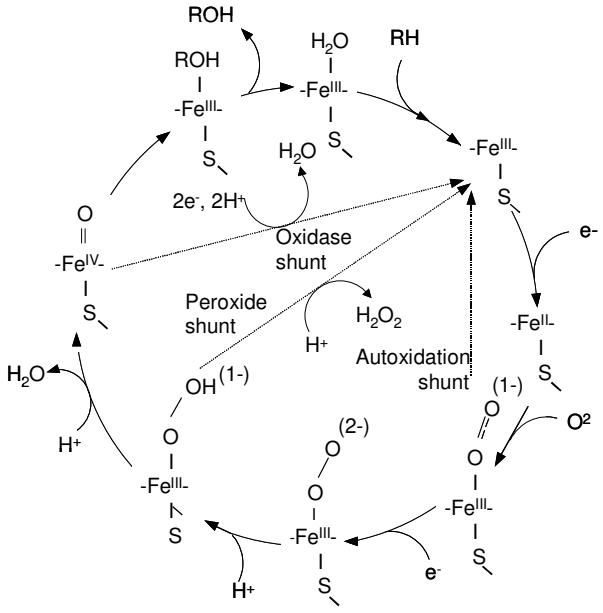

Figure 1.1. Overall catalytic mechanism for cytochrome P450 enzymes

1.2 P450 Enzymes in Biotechnology

The diversity of selective oxidation reactions catalyzed by P450 enzymes makes them attractive synthetic catalysts in biotechnology (*6*). The potential usefulness of P450 enzymes has been hindered by their mechanistic complexity, fragility, and inefficiency (*7*). As such, they are a prime target for groups seeking to develop industrially useful biocatalysts. The literature contains many successful examples of the engineering of P450 enzymes for enhanced stability, regioselectivity, and activity (*8-10*). Each of these studies chose a P450 scaffold to improve by rational or random mutagenesis. While these types of investigations can produce impressive results, it is often difficult to translate these results to the enhancement of the many thousands of other P450 enzymes in nature. It would be advantageous to develop general methods to improve P450 catalysis such that each activity or isoform does not need to be individually tailored to the task at hand. The identification of generally activating parameters could also, upon further mechanistic study, yield insights into the rational design of P450 enzymes.

The successful recombinant expression of human drug-metabolizing P450 enzymes in the early to mid nineties spawned a number of papers seeking to optimize the *in vitro* reconstitution of this complicated catalytic system (*11-14*). These papers resulted in general heuristics for conducting P450 reactions such as the inclusion of $MgCl_2$ with CYP3A4 or a lowered buffer concentration with CYP2C9 (*15*). Little is known, however, about the molecular origins of these heuristics. The simple manipulation of reaction conditions, which can improve catalytic activity by orders of magnitude, is a prime starting point for the identification of generally activating parameters. Moreover, from a research perspective, the flexibility of medium engineering allows access to a continuum of P450 function rather than the discrete mutants available in mutagenesis studies. This tunable range of P450 response offers a useful tool for the functional study of this complex system.

1.3 P450 Enzymes in the Pharmaceutical Industry

In humans, P450 enzymes are responsible for the majority of xenobiotic metabolism (*16*). Metabolism is accomplished by modifying lipophilic exogenous compounds to be more hydrophilic or to provide a reactive group for further functionalization so as to facilitate excretion. The enzymatic product can sometimes be more biologically active than the original compound. Codeine, for example, is enzymatically transformed into the active form via a P450 dealkylation that generates morphine (*17*). P450 enzymes are also capable of catalyzing the conversion of drug compounds into more toxic molecules. For example, the common analgesic, acetaminophen is metabolized by P450 enzymes to produce the hepatic toxin, N-acetyl-p-benzoquinone imine (*18*).

Seven P450 isoforms are responsible for the majority of oxidative drug metabolism in humans (*16*). Therefore, the potential for adverse drug-drug interactions is high. If two drugs are administered, both of which are metabolized by the same P450, each drug can act as an inhibitor for the other, drastically affecting the concentration profile seen by the body. It has been estimated that adverse drug-drug interactions are within a 95% confidence interval between the fourth and sixth leading cause of death for hospital patients in the United States (*19*). This fact compounded with the potential for

more toxic metabolic products clearly highlights the paramount importance of P450 enzymes to the pharmaceuticals industry in lead compound screening, where it is necessary to establish which P450 enzymes are responsible for a drug's metabolism to guide the administration of that drug to patients.

The rate of metabolism of a drug is, therefore, a key parameter used to evaluate potential candidates during drug development. *In vitro* experiments with P450 enzymes are used to estimate the metabolic stability, or rate of degradation, of a drug of interest. The standard methodology for metabolic stability measurements uses high-throughput liquid chromatography tandem mass spectrometry (LCMS/MS) (*20*). This technique requires expensive equipment and has limited throughput due to the inherently sequential nature of the separation and analysis steps. These problems limit the application of this technique to later stages of drug development where there are fewer compounds to evaluate.

1.4 Thesis Organization

The broad goal of my thesis is to develop and apply high-throughput methods to the study and application of P450 enzymes. I primarily focused on fluorescence intensity measurements. Fluorescence spectroscopy is advantageous in that it is highly sensitive such that small concentrations of fluorescent products can be selectively quantified against a heterogeneous background.

In the second chapter of this thesis, I investigate the effect of reaction conditions on P450 catalysis with the specific goal of determining whether an alteration in P450 selectivity accounts for the large variations in reaction rates observed in these systems. Regioselectivity and coupling as well as overall rates were monitored simultaneously. The results indicate that the selectivity of CYP1A2 mediated 3-cyanocoumarin oxidation was not significantly affected by temperature or potassium phosphate buffer concentration but was affected by pH and buffer type. This work was completed with the help of Jack Chai.

The work presented in the second chapter lead to the investigations in chapter three. I sought a more thorough kinetic investigation into the effect of different salt ions on P450 catalysis. The oxidation of a 3-cyanocoumarin substrate by CYP1A2 and CYP3A4 was measured as a function of concentration and ion type for twelve salts. We found that fluoride salts yielded the largest rate enhancements with both P450 isoforms. In addition, the kinetic parameters and noncompetitive intermolecular isotope effects were determined as a function of potassium fluoride and reductase content for the CYP1A2 oxidation of 7-methoxy-3-cyanocoumarin. These indicated the rate enhancements observed were primarily due to changes in k_{cat}. This work was completed with the help of Larry Gao and Michael Lin.

The fourth chapter is concerned with developing a more efficient method to screen lead compounds for P450 activity during drug development. A general approach is presented based on quantifying species in the P450 mechanism and solving the rate equation. This method is demonstrated with multiple P450 isoforms and with human liver microsomes. This method is anticipated to be generally useful to pharmaceutical industries to facilitate pre-clinical testing during drug development. This work was completed with the help of Eric Arnon and Jessica Ryan.

1.5 References

1. Ortiz de Montellano, P. R. (2005) *Cytochrome P450: Structure, Mechansim, and Biochemistry*, 3rd ed. ed., Plenum Press, New York.
2. Denisov, I. G., Makris, T. M., Sligar, S. G., and Schlichting, I. (2005) Structure and chemistry of cytochrome P450, *Chem Rev 105*, 2253-2277.
3. Guengerich, F. P. (2001) Common and uncommon cytochrome P450 reactions related to metabolism and chemical toxicity, *Chem Res Toxicol 14*, 611-650.
4. Makris, T. M., von Koenig, K., Schlichting, I., and Sligar, S. G. (2007) Alteration of P450 distal pocket solvent leads to impaired proton delivery and changes in heme geometry, *Biochemistry-Us 46*, 14129-14140.
5. Karuzina, I. I., Zgoda, V. G., Kuznetsova, G. P., Samenkova, N. F., and Archakov, A. I. (1999) Heme and apoprotein modification of cytochrome P450 2B4 during its oxidative inactivation in monooxygenase reconstituted system, *Free Radical Bio Med 26*, 620-632.
6. Julsing, M. K., Cornelissen, S., Buhler, B., and Schmid, A. (2008) Heme-iron oxygenases: powerful industrial biocatalysts?, *Current Opinion in Chemical Biology 12*, 177-186.
7. Urlacher, V. B., Lutz-Wahl, S., and Schmid, R. D. (2004) Microbial P450 enzymes in biotechnology, *Appl Microbiol Biot 64*, 317-325.
8. Glieder, A., Farinas, E. T., and Arnold, F. H. (2002) Laboratory evolution of a soluble, self-sufficient, highly active alkane hydroxylase, *Nat Biotechnol 20*, 1135-1139.
9. Joo, H., Lin, Z. L., and Arnold, F. H. (1999) Laboratory evolution of peroxide-mediated cytochrome P450 hydroxylation, *Nature 399*, 670-673.
10. Kumar, S., Sun, L., Muralidhara, B. K., Halpert, J. R., and Halpert, J. R. (2006) Engineering mammalian cytochrome P4502B1 by directed evolution for enhanced catalytic tolerance to temperature and dimethyl sulfoxide, *Protein Eng Des Sel 19*, 547-554.
11. Schenkman, J. B., Voznesensky, A. I., and Jansson, I. (1994) Influence of Ionic-Strength on the P450 Monooxygenase Reaction and Role of Cytochrome B(5) in the Process, *Archives of Biochemistry and Biophysics 314*, 234-241.
12. Yamazaki, H., Ueng, Y. F., Shimada, T., and Guengerich, F. P. (1995) Roles of Divalent Metal-Ions in Oxidations Catalyzed by Recombinant Cytochrome-P450 3a4 and Replacement of Nadph-Cytochrome P450 Reductase with Other Flavoproteins, Ferredoxin, and Oxygen Surrogates, *Biochemistry-Us 34*, 8380-8389.
13. Yamazaki, H., Gillam, E. M. J., Dong, M. S., Johnson, W. W., Guengerich, F. P., and Shimada, T. (1997) Reconstitution of recombinant cytochrome P450 2C10(2C9) and comparison with cytochrome P450 3A4 and other forms: Effects of cytochrome P450-P450 and cytochrome P450-b(5) interactions, *Archives of Biochemistry and Biophysics 342*, 329-337.
14. Davydov, D. R., Kariakin, A. A., Petushkova, N. A., and Peterson, J. A. (2000) Association of cytochromes P450 with their reductases: Opposite sign of the electrostatic interactions in P450BM-3 as compared with the microsomal 2B4 system, *Biochemistry-Us 39*, 6489-6497.

15. Yamazaki, H., and Shimada, T. (2006) Cytochrome P450 reconstitution systems, *Methods Mol Biol 320*, 61-71.
16. Wienkers, L. C., and Heath, T. G. (2005) Predicting in vivo drug interactions from in vitro drug discovery data, *Nature Reviews Drug Discovery 4*, 825-833.
17. Yue, Q. Y., Svensson, J. O., Alm, C., Sjoqvist, F., and Sawe, J. (1989) Codeine O-Demethylation Co-Segregates with Polymorphic Debrisoquine Hydroxylation, *Brit J Clin Pharmaco 28*, 639-645.
18. James, L. P., Mayeux, P. R., and Hinson, J. A. (2003) Acetaminophen-induced hepatotoxicity, *Drug Metab Dispos 31*, 1499-1506.
19. Lazarou, J., Pomeranz, B. H., and Corey, P. N. (1998) Incidence of adverse drug reactions in hospitalized patients - A meta-analysis of prospective studies, *Jama-J Am Med Assoc 279*, 1200-1205.
20. Youdim, K. A., and Saunders, K. C. (2010) A review of LC-MS techniques and high-throughput approaches used to investigate drug metabolism by cytochrome P450s, *J Chromatogr B 878*, 1326-1336.

CHAPTER 2

Simultaneous Measurement of CYP1A2 Activity, Regioselectivity, and Coupling: Implications for Environmental Sensitivity of Enzyme-Substrate Binding

2.1 Abstract

The cytochrome P450 (CYP) reaction mechanism often yields a broad array of coupled and uncoupled products from a single substrate. While it is well known that reaction conditions can drastically affect the rate of P450 catalysis, their effects on regioselectivity and coupling are not well characterized. To investigate such effects, the CYP1A2 oxidation of 7-ethoxymethoxy-3-cyanocoumarin (EOMCC) was examined as a function of buffer type, buffer concentration, pH, and temperature. A high-throughput, optical method was developed to simultaneously measure the rate of substrate depletion, NADPH depletion, and generation of the O-dealkylated product. Increasing the phosphate buffer concentration and temperature increased both the NADPH and EOMCC depletion rates by 6-fold, whereas coupling was constant at 7.9% and the regioselectivity of O-dealkylation to other coupled pathways was constant at 21.7%. Varying the buffer type and pH increased NADPH depletion by 2.5-fold and EOMCC depletion by 3.5-fold; however, neither coupling nor regioselectivity was constant, with variations of 14.4% and 21.6%, respectively. Because the enzyme-substrate binding interaction is a primary determinant of both coupling and regioselectivity, it is reasonable to conclude that ionic strength, as varied by the buffer concentration, and temperature alter the rate without affecting binding while buffer type and pH alter both.

2.2 Introduction

Human cytochrome P450 enzymes are important to the pharmaceutical and biotechnology industries due to their central role in drug metabolism, ability to generate and optimize lead compounds, and specialized oxidative abilities (*1*). The use of P450 enzymes in these capacities is complicated, however, by the wide variability of reaction rates observed in reconstituted *in vitro* systems (*2, 3*). This variability has been linked to the composition of the reaction medium (*4-7*). Because the P450 reaction mechanism is capable of generating multiple products, it is not known whether the variability in rates as a function of medium composition is accompanied by significant changes in selectivity.

Multiple P450 reaction products comprise two classes: coupled products where the electrons supplied by NADPH are coupled to substrate oxidation, and uncoupled products where the supplied electrons are lost to reduced oxygen species (*8*). Thus, there are two relevant reaction selectivities in P450 systems: the electron selectivity, commonly referred to as the coupling efficiency, which is the ratio of coupled to uncoupled product-generation rates; and the regioselectivity, which is the ratio of two different possible coupled product-generation rates. While it is well known that reaction conditions can affect P450 activity over orders of magnitude (*6*), it is currently unclear how P450 enzymes interact with environmental parameters such as pH, ionic strength, temperature, and small molecule additives to modulate these two selectivities. An improved understanding of these interactions could lead to more accurate *in vitro – in vivo*

metabolic correlations facilitating drug development (*3*), and assist in the development and optimization of synthetic schemes in the biotechnology sector (*2, 9*).

P450 regioselectivity is thought to be controlled by a combination of substrate positioning with respect to the active oxidant and the relative reactivity of different potential oxidation sites on the substrate (*10*). Regioselectivity of a very mobile substrate, one able to bind in many orientations, is likely governed primarily by the relative reactivity of the different chemical moieties in proximity to the heme. In contrast, regioselectivity of a tightly-bound substrate, one able to bind in only a few orientations, is presumably determined primarily by the relative occupancy of the different binding orientations (*11, 12*). Thus, an experimental parameter that alters regioselectivity would be expected to modify the occupancy or orientation of different binding modes of the substrate or differentially modify the reactivity of the substrate. The latter has been clearly demonstrated in kinetic isotope effect studies where the substitution of a heavy atom at one oxidation site of a mobile substrate can alter the regioselectivity toward reaction at other sites (*13*). Although previous studies have investigated the effect of buffer concentration, pH, and magnesium concentration on the regioselectivity of P450 reactions, the regulation of P450 selectivity by reaction conditions remains poorly understood. Buffer and magnesium concentrations have been found to alter catalytic activity but not regioselectivity, while pH has been shown to alter both (*14-17*).

Electron selectivity, or coupling, has also been linked to substrate-enzyme binding interactions. The structural complementarity of the substrate and P450 active site has been shown to be an important determinant of coupling (*18, 19*), where noncomplementarity results in improperly positioned water in the active site. These water molecules are thought to disrupt the proton delivery machinery required for the successive protonation of the ferric-peroxo intermediate, leading to a decrease in coupling efficiency (*20*). Guengerich points out that substrate dissociation rates can be large compared to catalytic rates, and coupling efficiency can be decreased by substrate dissociation after initiation of catalysis but before oxidation (*21*). Thus, a parameter that modifies the substrate-enzyme interaction and alters the off-rate or the packing of the active site is expected to affect coupling. Notably, an increase in buffer concentration was shown to increase coupling in the benzphetamine N-demethylation activity of CYP2B4 enriched rabbit liver microsomes (*22*); however, there are few studies in the literature examining the effect of reaction conditions on uncoupling.

In general, very little has been published on the relationship between environment and P450 selectivity. In particular, no previous studies have investigated the effect of reaction conditions on CYP1A2 regioselectivity or coupling. This void in the literature can be partially attributed to the large number of measurements needed to calculate these selectivities. To address this limitation, we developed a “one pot” method utilizing a single experimental technique, fluorescence intensity measurements, to simultaneously quantify activity, regioselectivity, and coupling. Depletion rates of NADPH and of an optically active substrate are analyzed in concert with the generation rate of at least one product. This method should be generally applicable to any substrate that is optically distinguishable from NADPH and one or more of its products. Here the method is demonstrated with the CYP1A2 oxidation of EOMCC to 7-hydroxy-3-cyanocoumarin (7HCC), which is a particularly challenging case study because the substrate’s fluorescence spectrum overlaps with the spectrum of NADPH. In addition, due to the

broad reactivity of cyanocoumarins (*23*), this model reaction can be used for many human drug metabolizing P450 enzymes allowing for a more direct comparison of selectivity data between isozymes.

To explore the relationship between environment and selectivity, the rates of NADPH depletion, EOMCC depletion, and 7HCC generation were measured as a function of buffer type, buffer concentration, pH, and temperature in the CYP1A2 oxidation of EOMCC, and the regioselectivity and coupling were compared under these conditions. The results indicate that both regioselectivity and coupling remain constant when temperature and buffer concentration are varied but are altered when buffer type and pH are varied. This indicates that temperature and ionic strength, as varied by buffer concentration, affect the rate of catalysis independent of the substrate-enzyme binding interaction while pH and buffer type affect both the rates and the binding interaction.

2.3 Materials and Methods

2.3.1 Materials

Piperonyl butoxide (PBO), potassium phosphate, nicotinamide adenine dinucleotide phosphate (NADPH), and acetonitrile were purchased from Sigma (St. Louis, MO). Microsomes from baculovirus-infected insect cells (Baculosomes) expressing human CYP1A2 and rabbit cytochrome P450 reductase (Lot 484429C), EOMCC, and 7HCC were purchased from Invitrogen (Carlsbad, Ca). All chemicals were used as received. All fluorescence data were acquired on a Spectramax M2 plate reader (Molecular Devices, Sunnyvale, CA).

2.3.2 Liquid Chromatography Mass Spectrometry

EOMCC oxidation reactions were conducted in 120 mM pH 8 potassium phosphate buffer with 25 nM CYP1A2 Baculosomes with or without the inhibitor PBO. Reactions were initiated with the simultaneous addition of NADPH and EOMCC to a concentration of 450 μM and 100 μM, respectively, to a final volume of 200 μL. Reactions were prepared and conducted at ambient temperature for 1 h and were quenched with 100 μL ice cold acetonitrile then centrifuged at 4°C for 10 min at 14000 g. Products were resolved using a reverse-phase Alltech Prevail C18 3μm 3.0x150 mm column with a 0.4 ml/min flow rate and a gradient of 10 – 80% acetonitrile over 40 min with a constant 0.05% concentration of formic acid. LCMS data were collected on an Agilent 1100 LC/MSD equipped with an electrospray ion source. Injections of inhibited, uninhibited, and no-protein control reactions were conducted separately in positive and negative mode. The quadrupole ion analyzer MS was operated with a fragmentor setting of 70 V, 3 kV capillary, 35 psig nebulizer pressure, and with N_2 drying gas set to 300°C and 9.5 L/min. LCMS/MS spectra were acquired using a ThermoFisher Scietific LTQ Orbitrap XL mass spectrometer in positive and negative modes. The flow rate was 0.2 mL/min and the mass spectrometer source parameters were used as follows: spray voltage, 3.0 kV; capillary temperature, 275°C; capillary voltage, 44 V (positive mode) and -50 V (negative mode); tube lens, 125 V (positive mode) and -120 V (negative mode).

2.3.3 Activity and Selectivity Assays

Six replicates were prepared with 25 nM CYP1A2 Baculosomes at the buffer condition noted in Figure 2.4 with and without 1 mM PBO. NADPH solutions were prepared fresh daily and the concentration was checked via absorbance using a molar extinction coefficient of 6.22 $mM^{-1}cm^{-1}$. Reactions were incubated for 20 min at the required temperature before initiation with the simultaneous addition of NADPH and EOMCC to 250 μM and 10 μM, respectively to a final volume of 100 μL.

The reaction was followed via fluorescence intensity measurements in a Spectramax M2 plate reader. Fluorescence intensity was simultaneously recorded at three excitation/emission wavelengths: 340 nm/460 nm, 340 nm/520 nm, 409 nm/460 nm. Models correlating fluorescence intensity with the concentration of EOMCC, NADPH, and 7HCC (Eqs. 1-3) were generated in JMP 5.1 using least-squares regression. The coefficients of Eqs. 1-3 were determined using on-plate standards at each reaction condition tested. The on-plate standards included a three-level, full factorial array of mixtures of NADPH and EOMCC to quantify fluorescence interactions. Significant model parameters were identified with the Backward Elimination method using a threshold P-value of 5%. Correlations typically took the form shown below.

$$RFU_{340/460} = a_1[EOMCC] + b_1[EOMCC][NADPH] + c_1[NADPH] + d_1[7HCC] \quad (1)$$

$$RFU_{340/520} = a_2[NADPH] + b_2[NADPH]^2 + c_2[EOMCC] + d_2[NADPH][7HCC] + e_2[7HCC] \quad (2)$$

$$RFU_{409/460} = a_3[7HCC] \quad (3)$$

The three coupled algebraic equations representing the dependence of fluorescence intensity on fluorophore concentration at each wavelength were solved for each data point in Matlab to yield concentration trajectories with time. The background reactions including PBO were subtracted out at each condition. The corrected time trajectory data were fit with a monoexponential function from which initial rates were calculated.

2.4 Results

2.4.1 Simultaneous *In Situ* Monitoring of EOMCC, 7HCC, and NADPH

The quantification of NADPH, EOMCC, and 7HCC via fluorescence intensity measurements is complicated in this system by the overlap of the fluorescence spectra of EOMCC and NADPH. While the emission of 7HCC is not affected by the presence of the other fluorophores, the emission maximum of NADPH (460 nm) overlaps with a strong signal from EOMCC (Fig. 2.1). However, at longer emission wavelengths, the NADPH signal is more distinct from that of the other fluorophores. The incorporation of emission data from both 460 nm and 520 nm upon excitation at 340 nm into a standard least-squares regression algorithm allowed for the generation of models correlating fluorescence intensity with fluorophore concentration. Correlation parameters were determined using on-plate standards at each condition tested and were validated by comparing the predicted and measured fluorescence intensities for mixtures of known concentrations of fluorophores, each yielding R^2 values greater than 0.98 indicating accurate fluorophore quantification (data not shown).

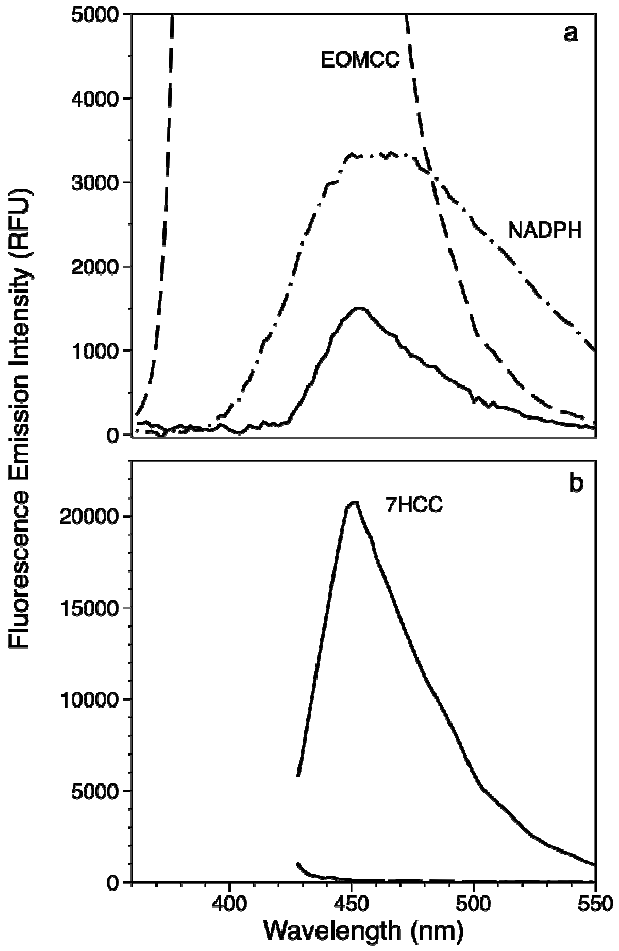

Figure 2.1. Fluorescence emission spectra of 250 μM NADPH, 10 μM EOMCC, and 1.2 μM 7HCC in 100 mM potassium phosphate at pH 7.5 upon excitation at (a) 340 nm and (b) 409 nm.

These correlation equations were solved to yield each fluorophore concentration as a function of time. Representative time trajectories of the three fluorophore concentrations are shown in Figure 2.2 for reactions with and without the P450 suicide inhibitor, PBO. Inhibition by PBO is hypothesized to occur via the formation of a stable carbene linkage to the heme iron blocking further catalysis by the P450 (*24*). Degradation of EOMCC and NADPH occurs in the presence of PBO, which can be attributed to both the instability of these molecules and to reactions with other components of the heterogeneous baculosome mixture. The background response of the inhibited system, which contains all components except functional P450, is thus crucial to isolate the contribution of only CYP1A2 from other reactions occurring in the system, such as the background oxidation of NADPH by the reductase. The absence of any 7HCC generation in the presence of PBO also indicates that, within the reaction mixture, only functional CYP1A2 can catalyze the conversion of EOMCC to 7HCC. Monoexponential fits were applied to the corrected time trace data and initial rates were calculated for the degradation of EOMCC, the generation of 7HCC, and the degradation of NADPH. The

exponential fit does not imply a mechanistic interpretation and was used because it closely reproduces the observed data (Fig. 2.2). Coupling is reported as the ratio of EOMCC depletion to NADPH depletion, and regioselectivity is indicated by the ratio of 7HCC generation to EOMCC depletion.

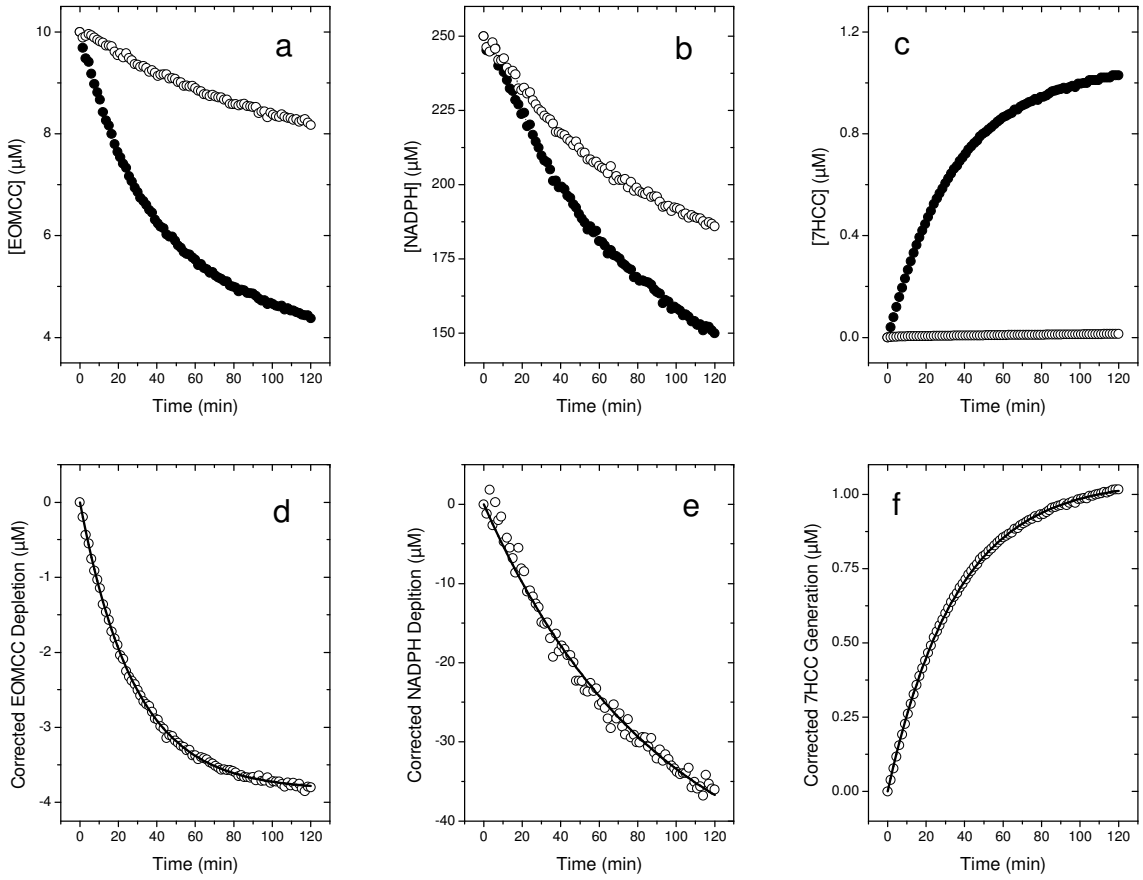

Figure 2.2. Representative data for the depletion of EOMCC (a) and NADPH (b), and the generation of 7HCC (c), in the presence (○) and absence (●) of the inhibitor PBO. The data with inhibition are subtracted from the data without inhibition to yield the corrected depletion of EOMCC (d), NADPH (e), and generation of 7HCC (f). A monoexponential curve is fit to the data and used to obtain an initial rate.

2.4.2 Multiple Coupled Products in the CYP1A2 Oxidation of EOMCC

To verify that the measured regioselectivity is governed by an enzyme-mediated process and not simply the rearrangement of a common intermediate into multiple products (*25*), the product profile was investigated with mass spectrometry. The reaction products of the CYP1A2 oxidation of EOMCC were analyzed with LCMS in the presence and absence of PBO. Product peaks were identifiable from background peaks as the product peaks disappeared in the presence of PBO. This was seen in three peaks eluting at 18.9 min, 23.6 min, and 30.5 min, which yielded major ions at *m/z* +236, -186, and -207 respectively (Fig. 2.3). Although the peak at 30.5 min exhibited a base peak at *m/z* -207, another product ion was present in this peak at a much lower abundance at *m/z* -

234. EOMCC eluted at 33.4 min and as expected exhibited a larger peak with PBO than in its absence. The substrate peak co-eluted with an EOMCC standard while the product at 23.6 min co-eluted with a 7HCC standard (data not shown). The small peak at 33.4 min in the *m/z* -186 chromatogram (Fig. 2.3B) arises from fragmentation of the substrate EOMCC during ionization.

To determine whether CYP1A2 oxidizes EOMCC at multiple sites, LCMS/MS analysis was conducted on EOMCC, 7HCC, and the unknown *m/z* +236 product (Fig. 2.4). Exact mass data and chemical formula predictions are given in Appendix 2.1. Unfortunately, the *m/z* -234 product could not be captured with LCMS/MS. The MS/MS fragmentation pattern of 7HCC (Fig. 2.4A) is characterized by the successive loss of either CO or CO_2 fragments as is common with coumarins (*26, 27*). The fragmentation of EOMCC exhibited a molecular ion at *m/z* +246 with a base peak at *m/z* +216 corresponding to a loss of 30 amu and a minor peak at *m/z* +188 corresponding to an overall loss of 56 amu. A comparison of the secondary fragmentation of the base peak from EOMCC and fragmentation of the molecular ion of 7-ethoxy-3-cyanocoumarin (EOCC) is shown in Figure 2.5. The similarities in the relative abundance and m/z of the fragments indicate that the molecular ion of EOMCC initially fragments with a loss of formaldehyde to generate the base peak at *m/z* +216 followed by a loss of ethylene to form the minor peak at *m/z* +188 (Fig. 2.6). The motif of a loss of 30 amu followed by a loss of 26 amu occurs via fragmentation in the 7-ethoxymethoxy moiety of the cyanocoumarin substrate. This motif is also seen in the MS/MS fragmentation of the unknown product ion *m/z* +236 (Fig. 2.4C) indicating that this product still contains an intact 7-ethoxymethoxy moiety and is generated from the oxidation of EOMCC at a different site than 7HCC. Thus, EOMCC occupies at least two binding orientations in the CYP1A2 active site with at least two sites of oxidation on the substrate.

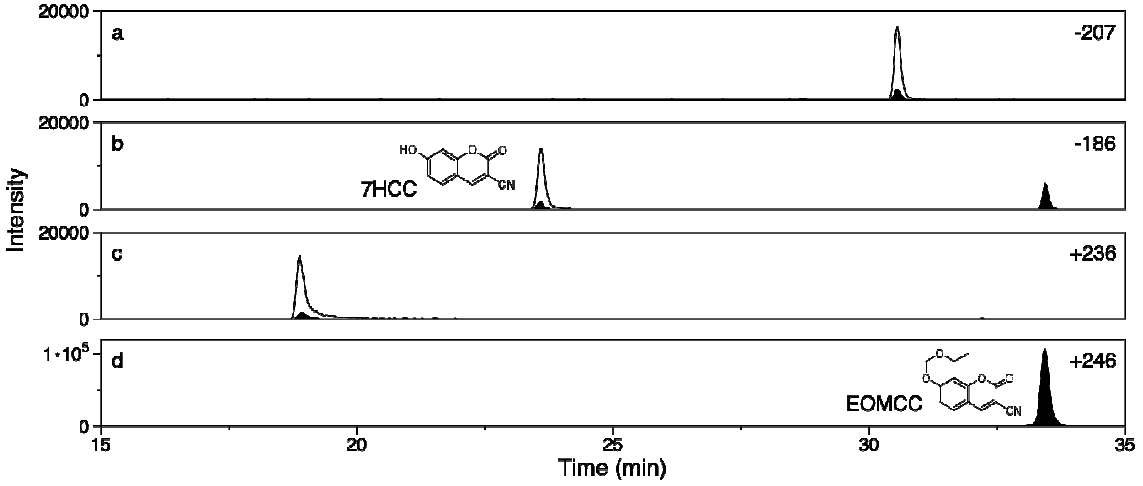

Figure 2.3. LCMS analysis of the reaction products of the CYP1A2 oxidation of EOMCC with single ion monitoring in negative mode of (a) *m/z* -207 and (b) *m/z* -186 and in positive mode of (c) *m/z* +236 and (d) *m/z* +246. The filled peaks are data from reactions including the suicide inhibitor, PBO, while the empty peaks are the response without inhibitor.

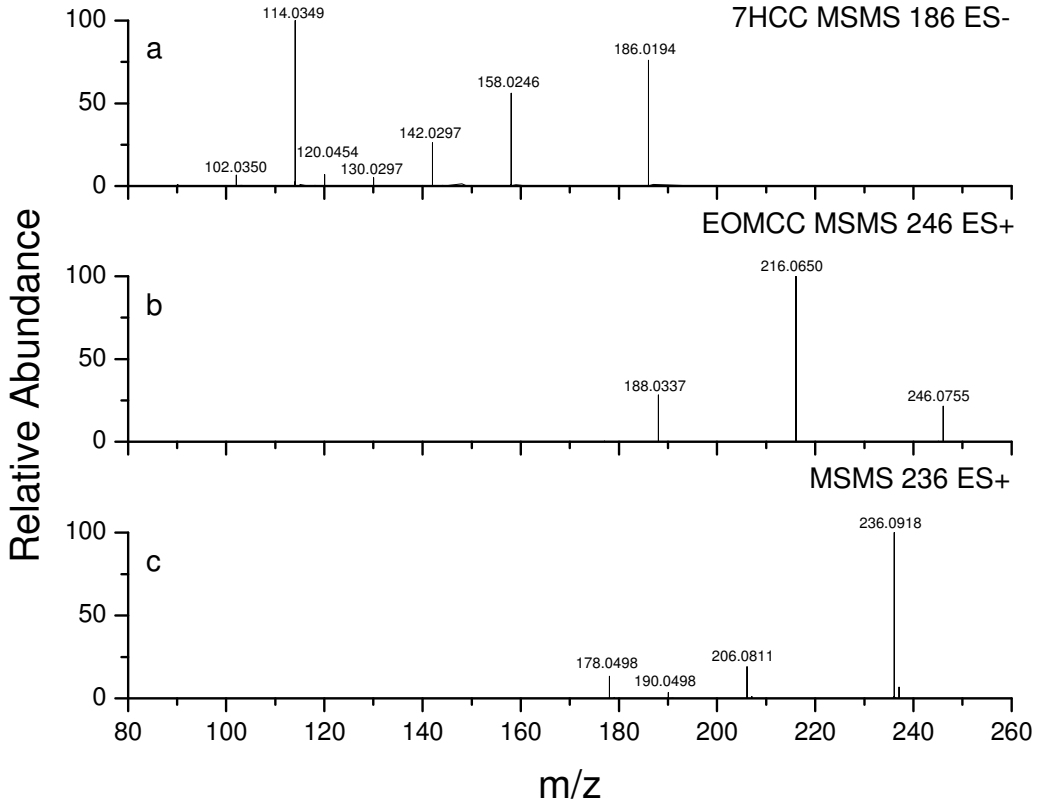

Figure 2.4. ESI-MS/MS fragmentations of (a) 7HCC and (b) EOMCC and (c) the product ion *m/z* +236

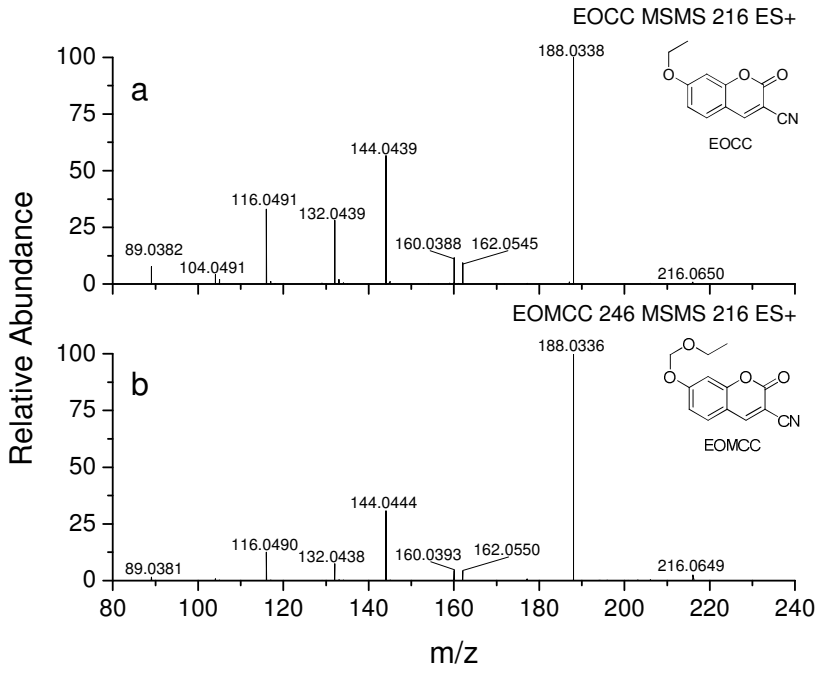

Figure 2.5. Positive mode ESI-MS/MS of (a) EOMCC with secondary ion fragmentation of the major peak at *m/z* +216 and of (b) EOCC.

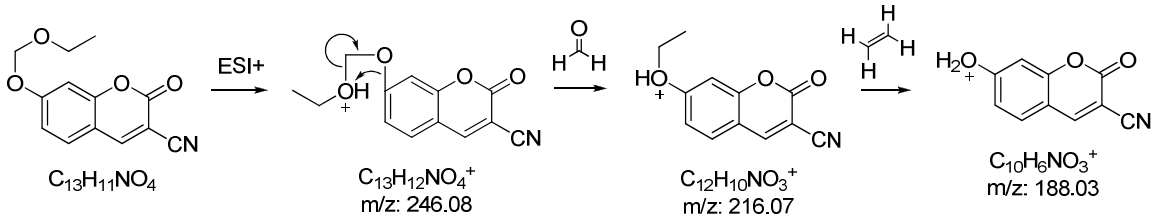

Figure 2.6. Proposed fragmentation pattern for EOMCC

2.4.3 Effect of Reaction Conditions on Activity and Selectivity

The initial rates of 7HCC generation (r_{7HCC}), EOMCC depletion ($-r_{EOMCC}$), and NADPH depletion ($-r_{NADPH}$) were measured in the reaction of CYP1A2 on EOMCC as a function of buffer type, buffer concentration, pH, and temperature (Fig. 2.7). Each rate increased with temperature, and appeared to be approaching a maximum at the highest achievable temperature of 45°C. Each rate also exhibited a maximum at a phosphate buffer concentration between 250 and 375 mM. A notable difference in rate was apparent, however, when varying the buffer type and pH, where $-r_{EOMCC}$ and $-r_{NADPH}$ both showed qualitatively similar behavior in Tris and phosphate buffers, yielding maxima at pH 6.7, while r_{7HCC} exhibited clearly distinct behavior in Tris and phosphate buffers. In Tris buffered systems, r_{7HCC} increased with decreasing pH down to the lowest assayed pH of 7.1. In phosphate buffered systems, r_{7HCC} exhibited a maximum at pH 7.7.

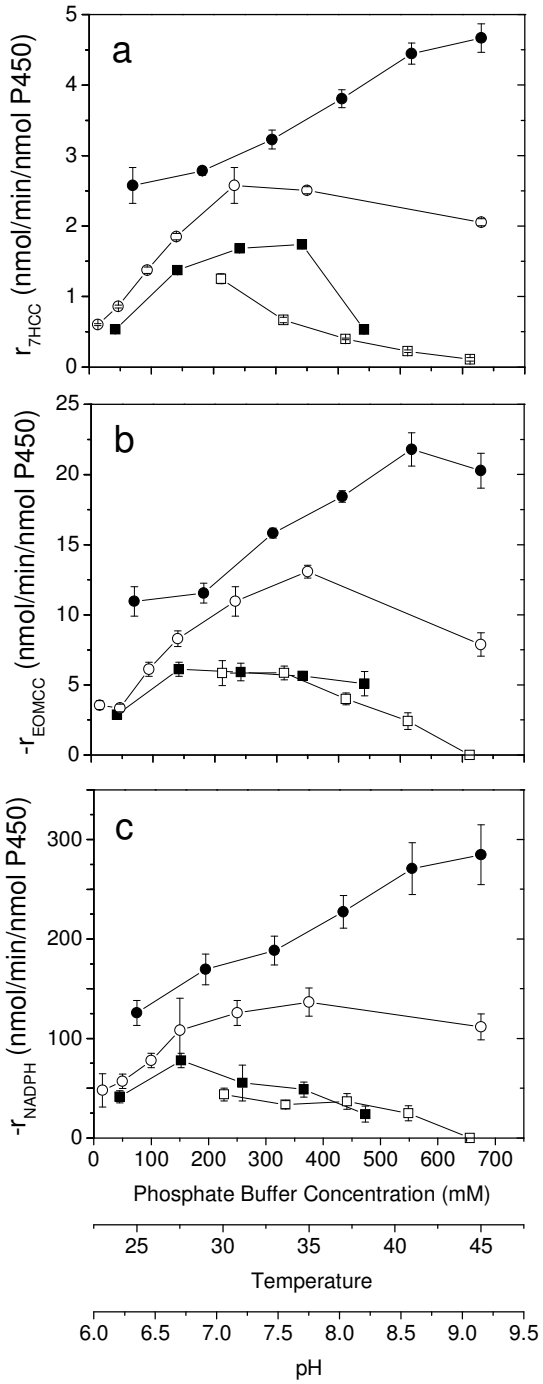

Figure 2.7. Initial rates of (a) 7HCC generation, (b) EOMCC depletion, and (c) NADPH depletion as a function of (□) pH in 100 mM Tris buffer at 25 °C, (■) pH in 100 mM phosphate buffer at 25 °C, (○) phosphate buffer concentration at pH 6.7 and 25 °C, and (●) temperature in 250 mM phosphate buffer at pH 6.7. A table of these rates can be found in Appendix 2.2.

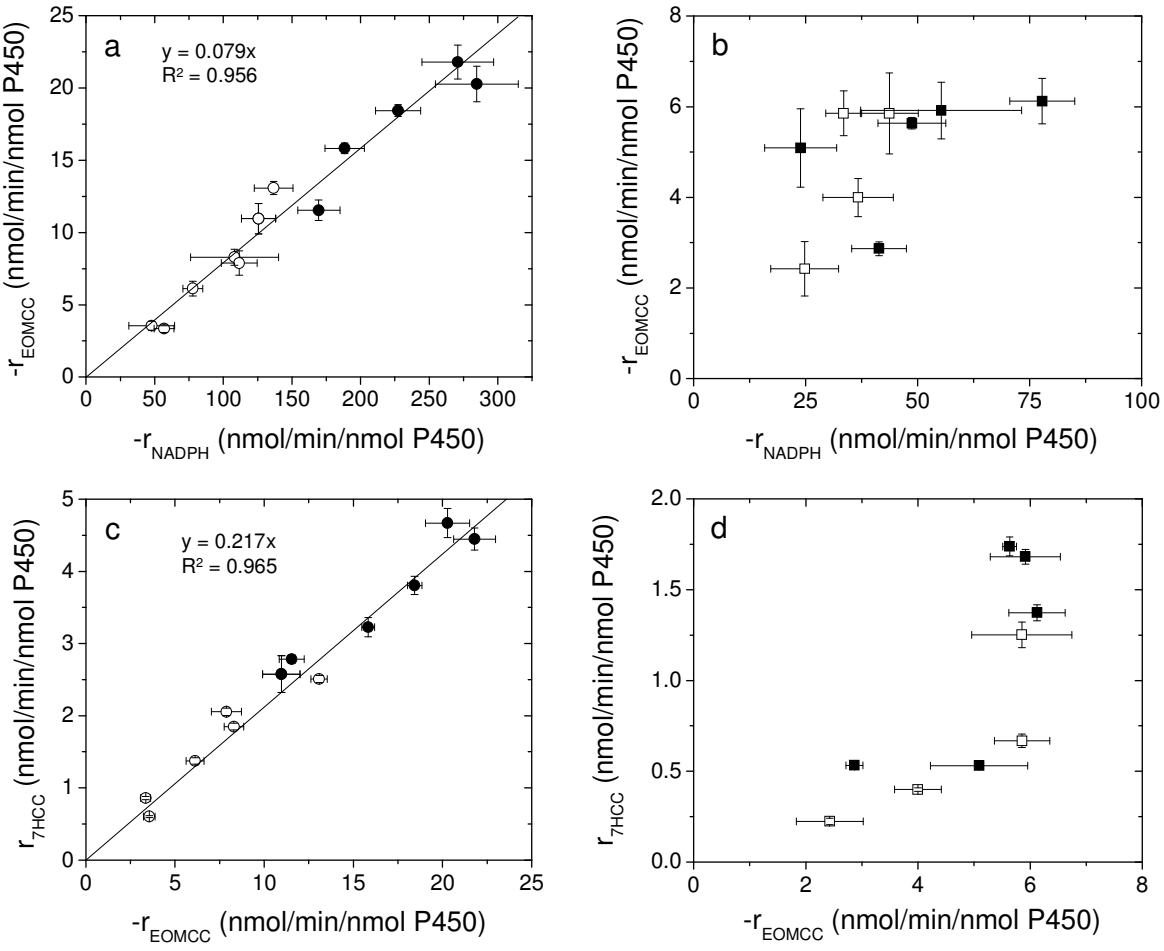

Figure 2.8. Correlation of the initial rate of EOMCC depletion, $-r_{EOMCC}$, with the initial rate of NADPH depletion, $-r_{NADPH}$, depicting the coupling efficiency (a,b), and of the initial rate of 7HCC generation, r_{7HCC}, with the initial rate of EOMCC depletion, r_{EOMCC}, depicting the regioselectivity (c,d). The data are from reactions varying the temperature (●) and phosphate buffer concentration (○), and the phosphate pH (■) and Tris pH (□). A table of these selectivity data can be found in Appendix 2.2.

A strong correlation was observed between $-r_{NADPH}$ and $-r_{EOMCC}$ as a function of both temperature and buffer concentration, indicating that coupling was not significantly changed by these parameters (Fig. 2.8A). Similarly, the correlation between $-r_{EOMCC}$ and r_{7HCC} indicates that these parameters also did not alter regioselectivity (Fig. 2.8C). These correlations, showing constant selectivity, contrast with the 6-fold change in activity observed with a variation in temperature and buffer concentration at pH 6.7. The selectivity results are illustrated in scheme 2.1 where 7.9% of the reducing equivalents from NADPH were used for coupled catalysis and 1.7% of the overall reducing equivalents or 21.7% of the depleted EOMCC was used to generate 7HCC via O-dealkylation. Conversely, despite the qualitatively similar behavior of $-r_{EOMCC}$ and $-r_{NADPH}$ as a function of buffer type and pH, much weaker correlations were observed for both coupling and regioselectivity as a function of these parameters (Fig. 2.8B,D). Coupling and regioselectivity varied by 14.4% and 21.6%, respectively. It is important to mention that standard assays containing known amounts of all three fluorophores indicated that the fluorescence responses are not inherently correlated (data not shown). Thus the selectivity trends found in this study are not a result of spurious correlations.

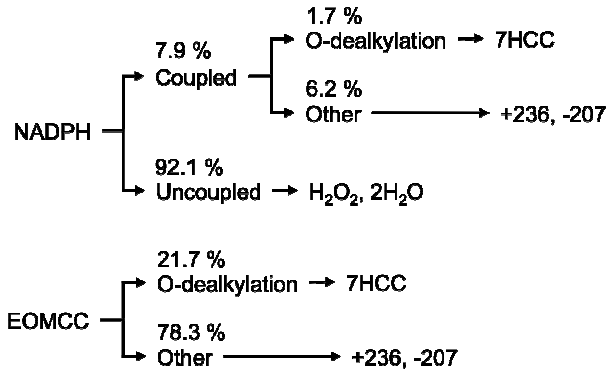

Scheme 2.1. Selectivity of electron (upper) and substrate (lower) utilization in the oxidation of EOMCC by CYP1A2 in pH 6.7 phosphate buffer

2.5 Discussion

Medium engineering offers a useful tool for the investigation of P450 function because a tunable range of P450 responses can be accessed by simply varying the reaction conditions. The practical utility and potential generality of medium engineering has been demonstrated by the large rate increases achieved with optimized P450 reconstitution procedures (*6*). The current study seeks to investigate the connection between environment and P450 selectivity using a novel method to simultaneously measure activity, coupling, and regioselectivity.

LCMS analysis verified the presence of multiple coupled products and identified three product peaks. MS/MS analysis revealed an intact ethoxymethoxy moiety on the product eluting at 18.9 min indicating this product is generated via a distinct mechanism from the O-dealkylation product, 7HCC. Furthermore, the mass and formula of the *m/z* +236 product are consistent with a P450 mediated 3,4-epoxidation followed by a ring opening and decarboxylation similar to the reaction of CYP1A2 with coumarin (*28, 29*). Interestingly, another product eluting over 11 minutes later at 30.5 min was identified

with a major peak in negative mode LCMS at *m/z* -207 and a minor peak at *m/z* -234. This product could not be captured in LCMS/MS analysis; nonetheless, the mass is also consistent with an epoxidation and decarboxylation reaction generating the *m/z* -234 product that presumably fragments during ionization to form the major *m/z* -207 peak. Although, the +236 and -234 products exhibit different elution times and different ionization behavior, their similar masses suggest that they may arise from the decarboxylation of a common intermediate generated from a common substrate-binding mode. Overall, however, the MS/MS data indicate the presence of two distinct products that are produced from at least two catalytically relevant binding modes for EOMCC in the CYP1A2 active site. Thus, the regioselectivity determined in this system reflects the relative binding of EOMCC in multiple orientations and the oxidation of multiple sites on the substrate. The presence of multiple binding orientations, indicated by the oxidation of multiple sites on the molecule, is typical of CYP1A2 substrates with caffeine (*30*) and phenacetin (*31*) being well-studied examples.

By varying the buffer type, buffer concentration, pH, and temperature in the CYP1A2 oxidation of EOMCC, a 10-fold range of rates was accessed with the highest activity found at pH 6.7 in 250 mM phosphate buffer at 45 °C. Ionic strength is typically varied by varying the buffer concentration, with maximum product generation rates occurring between 50 and 300 mM (*5, 6*). Although exceptions have been found for this trend (*5*), all measured rates in the present study increased with increasing phosphate buffer concentration to a maximum between 250 and 375 mM potassium phosphate. An increase in the measured rates was also observed with temperature between 25°C and 45°C, the highest temperature setting available on the instrument. The denaturation temperature of human CYP1A2 in reconstituted membranes reportedly varied with membrane composition between 40°C and 50°C (*32*). This matched the behavior observed in the present work where the measured rates showed signs of leveling off at 45°C.

The measured r_{7HCC} was higher in phosphate than in Tris-buffered systems. Similarly, Mäenpää et al. reported higher product generation rates in phosphate versus Tris buffered systems for the midazolam hydroxylation of human liver microsomes (*16*). Other studies, however, have shown similar P450 activity in different buffers. For example, the 7-pentoxyresorufin O-dealkylation activity of rabbit CYP1A2 was comparable in sodium phosphate, potassium acetate, and HEPES (*33*). Interestingly, $-r_{NADPH}$ and $-r_{EOMCC}$ showed similar behavior in phosphate and Tris buffered systems, demonstrating that buffer type can alter both the rate of product generation and of substrate depletion independently. Since all three measured rates increased similarly with increasing ionic strength, as varied by the phosphate buffer concentration, the inherently larger ionic strength of phosphate compared to Tris is not an adequate argument to explain the different behavior of r_{7HCC} compared to $-r_{EOMCC}$ and $-r_{NADPH}$ in these two buffers. P450 reactions are also known to be differentially affected by pH with different product generation optima for different isoform/substrate combinations (*14, 34, 35*). The current study extends this result to show that substrate depletion and product generation can exhibit disparate pH optima.

A strong correlation was observed between $-r_{EOMCC}$ and $-r_{NADPH}$ as a function of temperature and phosphate buffer concentration (Fig. 2.8A) indicating that coupling is not significantly affected by these variables. CYP1A2 oxidation of EOMCC was 92.1%

uncoupled for all buffer concentrations and temperatures at pH 6.7. Similarly high uncoupling percentages have been found for the CYP1A2 oxidation of phenacetin (*31, 36*) and of 7-ethoxycoumarin (*37*) and for other human P450 enzymes (*38-40*). A much weaker correlation between $-r_{EOMCC}$ and $-r_{NADPH}$ was found as a function of buffer type and pH (Fig 2.8B) indicating that coupling is altered by these variables. To the best of our knowledge this is the first investigation of P450 coupling as a function of buffer type, pH, or temperature. However Schenkman et al. observed an increase in the coupling of the benzphetamine N-demethylation activity of CYP2B4 enriched rabbit liver microsomes with increasing phosphate buffer concentration (*22*). This observation contrasts with our own data where buffer concentration did not alter coupling, suggesting that P450 coupling may be differentially regulated by reaction conditions for different P450 systems.

Similarly, regioselectivity was also not significantly altered by temperature or phosphate buffer concentration (Fig 2.8C). It was found that 21.7% of the oxidized EOMCC was used to generate the O-dealkylation product 7HCC in pH 6.7 phosphate solution. While no previous study has investigated the effect of temperature on regioselectivity, similar trends with buffer concentration have been observed (*14, 16*). Buffer concentration did not alter the ratio of several testosterone metabolites from purified rat CYP2A1, CYP2B1, and CYP2C11 (*14*) or of midazolam metabolites from human liver microsomes (*16*), consistent with our findings that regioselectivity was insensitive to buffer concentration. However, a change in regioselectivity with pH was reported for the oxidation of testosterone by rat CYP2A1, CYP2B1, and CYP2C11 (*14*) and for cyclosporine metabolism of human CYP3A4 (*15*). Likewise, our results revealed a change in regioselectivity with pH and additionally with buffer type. In light of previous literature on several P450 isoforms and substrates, these data suggest that ionic strength, as varied by buffer concentration, may generally affect the activity of a P450 reaction but not the regioselectivity, while pH may affect both. However, further work with additional P450 isoforms and substrates is needed to confirm this conclusion.

It is relevant to emphasize that 7HCC is a minor product in the overall oxidation of EOMCC by CYP1A2. This low regioselectivity toward O-dealkylation suggests that studies employing 7-alkoxy-3-cyanocoumarin substrates as convenient fluorescent probes for CYP1A2 activity are measuring only a fraction of the reaction products. A further elaboration of the product profile of commonly used coumarin substrates would be a valuable contribution to the literature, especially in light of our current finding that 7HCC accounts for only 21.7% of the substrate depletion.

Because regioselectivity and coupling are governed by enzyme-substrate binding interactions and neither temperature nor buffer concentration altered regioselectivity or coupling, it follows that these parameters do not alter the enzyme-substrate binding interactions. Variations in P450 function with buffer concentration have been previously attributed to the resulting variation in ionic strength and not to specific effects of phosphate ions (*5, 14, 16, 22, 41*). Although ion-specific effects are known in P450 systems (*7, 42, 43*), the correlation of phosphate buffer effects with ionic strength effects is supported by the similar activity trends observed in the CYP1A2 de-ethylation of 7-ethoxyresorufin and 7-ethoxycoumarin as a function of phosphate buffer and sodium chloride concentration (*41*). Variations in P450 function with ionic strength have been attributed to an alteration of the P450 – reductase interaction (*5, 22*) or the heteromeric

oligomerization state (*33, 44*), both of which have been shown to be mediated by ionic interactions (*33, 44-46*). In addition, the reduction of cytochrome c by P450 reductase, studied as a function of pH and ionic strength, yielded activity maxima at pH 7.5 (*47*) and an ionic strength of 500 mM (*48*), similar to the behavior observed in the current work. It is conceivable that selectivity is regulated by the enzyme-substrate binding interaction, which controls substrate positioning, while activity is regulated by the P450-reductase interaction, which controls the flow of electrons to the P450.

Ionic strength, as varied by sodium chloride concentration, has been shown to alter the structure of rabbit CYP1A2 as measured by circular dichroism (*41*). It is interesting that this change in structure could accompany a large change in activity without also perturbing the active site and altering the substrate binding interactions relevant to selectivity. Schrag et al., however, observed constant selectivity in the presence of a structural perturbation of the active site in the CYP3A4 metabolism of triazolam. Regioselectivity was unaffected by a change in active site topography induced by magnesium ions (*17*). Overall, it is clear that more work is needed to understand the complex interactions between environmental parameters and P450 function.

In conclusion, mass spectrometry was used to confirm the existence of multiple coupled catalytic modes for the CYP1A2 oxidation of EOMCC in addition to the standard uncoupled modes. An *in situ* optical method was developed to monitor the activity and selectivity of human drug metabolizing enzymes and demonstrated on a cyanocoumarin substrate. This method is anticipated to be a useful tool for protein engineering studies seeking to understand and control the influence of reaction conditions on P450 function. While the activity of CYP1A2 in this work was found to vary over 10-fold as a function of buffer type, buffer concentration, pH, and temperature, the regioselectivity and coupling efficiency were effectively constant with buffer concentration and temperature but varied with buffer type and pH. Future work will investigate the generality of these results with other P450 isoforms with the aim of developing general heuristics relating P450 selectivity and environmental parameters.

2.6 Acknowledgement

We thank Rita Nichiporuk and Ulla Anderson for assistance with the mass spectrometry experiments and data interpretation, and Jessica Ryan and Elizabeth Schneider for helpful discussions. This work was supported by the National Science Foundation and the National Institutes of Health.

2.7 References

1. Ortiz de Montellano, P. R. (2005) *Cytochrome P450: Structure, Mechansim, and Biochemistry*, 3rd ed. ed., Plenum Press, New York.
2. Julsing, M. K., Cornelissen, S., Buhler, B., and Schmid, A. (2008) Heme-iron oxygenases: powerful industrial biocatalysts?, *Current Opinion in Chemical Biology 12*, 177-186.
3. Wienkers, L. C., and Heath, T. G. (2005) Predicting in vivo drug interactions from in vitro drug discovery data, *Nature Reviews Drug Discovery 4*, 825-833.
4. Gillam, E. M. J., Baba, T., Kim, B. R., Ohmori, S., and Guengerich, F. P. (1993) Expression of Modified Human Cytochrome-P450 3a4 in Escherichia-Coli and

Purification and Reconstitution of the Enzyme, *Archives of Biochemistry and Biophysics 305*, 123-131.

5. Yamazaki, H., Gillam, E. M. J., Dong, M. S., Johnson, W. W., Guengerich, F. P., and Shimada, T. (1997) Reconstitution of recombinant cytochrome P450 2C10(2C9) and comparison with cytochrome P450 3A4 and other forms: Effects of cytochrome P450-P450 and cytochrome P450-b(5) interactions, *Archives of Biochemistry and Biophysics 342*, 329-337.
6. Yamazaki, H., and Shimada, T. (2006) Cytochrome P450 reconstitution systems, *Methods Mol Biol 320*, 61-71.
7. Yamazaki, H., Ueng, Y. F., Shimada, T., and Guengerich, F. P. (1995) Roles of Divalent Metal-Ions in Oxidations Catalyzed by Recombinant Cytochrome-P450 3a4 and Replacement of Nadph-Cytochrome P450 Reductase with Other Flavoproteins, Ferredoxin, and Oxygen Surrogates, *Biochemistry-Us 34*, 8380-8389.
8. Sigel, A., Sigel, H., and Sigel, R. K. O. (2007) *The Ubiquitous Roles of Cytochrome P450 Proteins*, John Wiley & Sons, Ltd., Chichester, U.K.
9. Gillam, E. M. J. (2007) Extending the capabilities of nature's most versatile catalysts: Directed evolution of mammalian xenobiotic-metabolizing P450s, *Archives of Biochemistry and Biophysics 464*, 176-186.
10. White, R. E., Mccarthy, M. B., Egeberg, K. D., and Sligar, S. G. (1984) Regioselectivity in the Cytochromes-P-450 - Control by Protein Constraints and by Chemical Reactivities, *Archives of Biochemistry and Biophysics 228*, 493-502.
11. Seifert, A., Tatzel, S., Schmid, R. D., and Pleiss, J. (2006) Multiple molecular dynamics simulations of human P450 monooxygenase CYP2C9: The molecular basis of substrate binding and regioselectivity toward warfarin, *Proteins-Structure Function and Bioinformatics 64*, 147-155.
12. Wester, M. R., Johnson, E. F., Marques-Soares, C., Dansette, P. M., Mansuy, D., and Stout, C. D. (2003) Structure of a substrate complex of mammalian cytochrome P4502C5 at 2.3 angstrom resolution: Evidence for multiple substrate binding modes, *Biochemistry-Us 42*, 6370-6379.
13. Miwa, G. T., and Lu, A. Y. H. (1987) Kinetic Isotope Effects and Metabolic Switching in Cytochrome-P450-Catalyzed Reactions, *Bioessays 7*, 215-219.
14. Gemzik, B., Halvorson, M. R., and Parkinson, A. (1990) Pronounced and Differential-Effects of Ionic-Strength and Ph on Testosterone Oxidation by Membrane-Bound and Purified Forms of Rat-Liver Microsomal Cytochrome-P-450, *Journal of Steroid Biochemistry and Molecular Biology 35*, 429-440.
15. Hermann, M., Kase, E. T., Molden, E., and Christensen, H. (2006) Evaluation of microsomal incubation conditions on CYP3A4-mediated metabolism of cyclosporine a by a statistical experimental design, *Current Drug Metabolism 7*, 265-271.
16. Maenpaa, J., Hall, S. D., Ring, B. J., Strom, S. C., and Wrighton, S. A. (1998) Human cytochrome P450 3A (CYP3A) mediated midazolam metabolism: the effect of assay conditions and regioselective stimulation by alpha-naphthoflavone, terfenadine and testosterone, *Pharmacogenetics 8*, 137-155.
17. Schrag, M. L., and Wienkers, L. C. (2000) Topological alteration of the CYP3A4 active site by the divalent cation Mg2+, *Drug Metab Dispos 28*, 1198-1201.

18. Loida, P. J., and Sligar, S. G. (1993) Molecular Recognition in Cytochrome-P-450 - Mechanism for the Control of Uncoupling Reactions, *Biochemistry-Us 32*, 11530-11538.
19. Makris, T. M., von Koenig, K., Schlichting, I., and Sligar, S. G. (2007) Alteration of P450 distal pocket solvent leads to impaired proton delivery and changes in heme geometry, *Biochemistry-Us 46*, 14129-14140.
20. Denisov, I. G., Makris, T. M., Sligar, S. G., and Schlichting, I. (2005) Structure and chemistry of cytochrome P450, *Chem Rev 105*, 2253-2277.
21. Guengerich, F. P. (2004) Cytochrome p450: What have we learned and what are the future issues?, *Drug Metabolism Reviews 36*, 159-197.
22. Schenkman, J. B., Voznesensky, A. I., and Jansson, I. (1994) Influence of Ionic-Strength on the P450 Monooxygenase Reaction and Role of Cytochrome B(5) in the Process, *Archives of Biochemistry and Biophysics 314*, 234-241.
23. Stresser, D. M., Turner, S. D., Blanchard, A. P., Miller, V. P., and Crespi, C. L. (2002) Cytochrome P450 fluorometric substrates: identification of isoform-selective probes for rat CYP2D2 and human CYP3A4, *Drug Metab Dispos 30*, 845-852.
24. Murray, M. (2000) Mechanisms of inhibitory and regulatory effects of methylenedioxyphenyl compounds on cytochrome P450-dependent drug oxidation, *Current Drug Metabolism 1*, 67-84.
25. Guengerich, F. P. (2001) Common and uncommon cytochrome P450 reactions related to metabolism and chemical toxicity, *Chem Res Toxicol 14*, 611-650.
26. Concannon, S., Ramachandran, V. N., and Smyth, W. F. (2000) A study of the electrospray ionisation of selected coumarin derivatives and their subsequent fragmentation using an ion trap mass spectrometer, *Rapid Communications in Mass Spectrometry 14*, 1157-1166.
27. Timonen, J., Aulaskari, P., Hirva, P., and Vainiotalo, P. (2009) Negative ion electrospray ionization mass spectrometry and computational studies on substituted 7-hydroxycoumarins, *European Journal of Mass Spectrometry 15*, 595-603.
28. Born, S. L., Caudill, D., Fliter, K. L., and Purdon, M. P. (2002) Identification of the cytochromes P450 that catalyze coumarin 3,4-epoxidation and 3-hydroxylation, *Drug Metab Dispos 30*, 483-487.
29. Born, S. L., Rodriguez, P. A., Eddy, C. L., and LehmanMcKeeman, L. D. (1997) Synthesis and reactivity of coumarin 3,4-epoxide, *Drug Metab Dispos 25*, 1318-1323.
30. Regal, K. A., Kunze, K. L., Peter, R. M., and Nelson, S. D. (2005) Oxidation of caffeine by CYP1A2: Isotope effects and metabolic switching, *Drug Metab Dispos 33*, 1837-1844.
31. Yun, C. H., Miller, G. P., and Guengerich, F. P. (2000) Rate-determining steps in phenacetin oxidations by human cytochrome P450 1A2 and selected mutants, *Biochemistry-Us 39*, 11319-11329.
32. Ahn, T., Yun, C. H., and Oh, D. B. (2005) Involvement of nonlamellar-prone lipids in the stability increase of human cytochrome P450 1A2 in reconstituted membranes, *Biochemistry-Us 44*, 9188-9196.

33. Kelley, R. W., Reed, J. R., and Backes, W. L. (2005) Effects of ionic strength on the functional interactions between CYP2134 and CYP1A2, *Biochemistry-Us 44*, 2632-2641.
34. Delaforge, M., Ladam, P., Bouille, G., Benarous, J. G., Jaouen, M., and Girault, J. P. (1992) Ph Effects on the N-Demethylation and Formation of the Cytochrome-P-450 Iron-Ii Nitrosoalkane Complex for Erythromycin Derivatives, *Chemico-Biological Interactions 85*, 215-227.
35. Hutzler, J. M., Powers, F. J., Wynalda, M. A., and Wienkers, L. C. (2003) Effect of carbonate anion on cytochrome P450 2D6-mediated metabolism in vitro: the potential role of multiple oxygenating species, *Archives of Biochemistry and Biophysics 417*, 165-175.
36. Huang, Q. B., and Szklarz, G. D. (2010) Significant Increase in Phenacetin Oxidation on L382V Substitution in Human Cytochrome P450 1A2, *Drug Metab Dispos 38*, 1039-1045.
37. Mayuzumi, H., Sambongi, C., Hiroya, K., Shimizu, T., Tateishi, T., and Hatano, M. (1993) Effect of Mutations of Ionic Amino-Acids of Cytochrome-P450-1a2 on Catalytic Activities toward 7-Ethoxycoumarin and Methanol, *Biochemistry-Us 32*, 5622-5628.
38. Fang, X. J., Kobayashi, Y., and Halpert, J. R. (1997) Stoichiometry of 7-ethoxycoumarin metabolism by cytochrome P450 2B1 wild-type and five active-site mutants, *Febs Letters 416*, 77-80.
39. Locuson, C. W., Gannett, P. M., and Tracy, T. S. (2006) Heteroactivator effects on the coupling and spin state equilibrium of CYP2C9, *Archives of Biochemistry and Biophysics 449*, 115-129.
40. Perret, A., and Pompon, D. (1998) Electron shuttle between membrane-bound cytochrome P450 3A4 and b(5) rules uncoupling mechanisms, *Biochemistry-Us 37*, 11412-11424.
41. Yun, C. H., Song, M., Ahn, T., and Kim, H. (1996) Conformational change of cytochrome p450 1A2 induced by sodium chloride, *J Biol Chem 271*, 31312-31316.
42. Kim, J. S., Ahn, T., Yim, S. K., and Yun, C. H. (2002) Differential effect of copper (II) on the cytochrome P450 enzymes and NADPH-cytochrome P450 reductase: Inhibition of cytochrome P450-catalyzed reactions by copper (II) ion, *Biochemistry-Us 41*, 9438-9447.
43. Kim, J. S., and Yun, C. H. (2005) Inhibition of human cytochrome P450 3A4 activity by zinc(II) ion, *Toxicology Letters 156*, 341-350.
44. Kelley, R. W., Cheng, D. M., and Backes, W. L. (2006) Heteromeric complex formation between CYP2E1 and CYP1A2: Evidence for the involvement of electrostatic interactions, *Biochemistry-Us 45*, 15807-15816.
45. Davydov, D. R., Kariakin, A. A., Petushkova, N. A., and Peterson, J. A. (2000) Association of cytochromes P450 with their reductases: Opposite sign of the electrostatic interactions in P450BM-3 as compared with the microsomal 2B4 system, *Biochemistry-Us 39*, 6489-6497.
46. Backes, W. L., and Kelley, R. W. (2003) Organization of multiple cytochrome P450s with NADPH-cytochrome P450 reductase in membranes, *Pharmacology & Therapeutics 98*, 221-233.

47. Sem, D. S., and Kasper, C. B. (1993) Enzyme-Substrate Binding Interactions of Nadph-Cytochrome-P-450 Oxidoreductase Characterized with Ph and Alternate Substrate Inhibitor Studies, *Biochemistry-Us 32*, 11539-11547.
48. Sem, D. S., and Kasper, C. B. (1995) Effect of Ionic-Strength on the Kinetic Mechanism and Relative Rate Limitation of Steps in the Model Nadph-Cytochrome P450 Oxidoreductase Reaction with Cytochrome-C, *Biochemistry-Us 34*, 12768-12774.

Appendix 2.1 Exact Mass and Formula Predictions for MS/MS Data

	Abundance	obsd m/z	calcd m/z	error (ppm)	Formula
7HCC MSMS	6.59	102.0350	102.0349	0.8	C_7H_4N
186 ES-	100.00	114.0349	114.0349	-0.2	C_8H_4N
	6.96	120.0454	120.0455	-0.7	C_7H_5NO
	4.89	130.0297	130.0298	-1.1	C_8H_4NO
	26.11	142.0297	142.0298	-1.0	C_9H_4NO
	56.05	158.0246	158.0248	-1.0	$C_9H_4NO_2$
	75.92	186.0194	186.0197	-1.4	$C_{10}H_4NO_3$
MSMS 236	13.34	178.0498	178.0499	-0.4	$C_9H_8NO_3$
ES+	3.43	190.0498	190.0499	-0.4	$C_{10}H_8NO_3$
	19.04	206.0812	206.0812	0.2	$C_{11}H_{12}NO_3$
	100.00	236.0919	236.0917	0.7	$C_{12}H_{14}NO_4$
EOMCC	28.26	188.0337	188.0342	-2.8	$C_{10}H_6NO_3$
MSMS 246	100.00	216.0650	216.0655	-2.4	$C_{12}H_{10}NO_3$
ES+	21.51	246.0755	246.0761	-2.4	$C_{13}H_{12}NO_4$

Table 2.1. Exact mass and formula predictions for the MS/MS data in Figure 2.4.

	Abundance	obsd m/z	calcd m/z	error (ppm)	Formula
EOCC MSMS	7.68	89.0382	89.0386	-4.2	C_7H_5
216 ES+	4.17	104.0491	104.0495	-3.6	C_7H_6N
	1.92	105.0331	105.0335	-3.7	C_7H_5O
	32.99	116.0491	116.0495	-3.2	C_8H_6N
	28.08	132.0439	132.0444	-3.7	C_8H_6NO
	56.62	144.0439	144.0444	-3.4	C_9H_6NO
	11.60	160.0388	160.0393	-3.1	$C_9H_6NO_2$
	9.33	162.0545	162.0550	-2.8	$C_9H_8NO_2$
	100.00	188.0338	188.0342	-2.2	$C_{10}H_6NO_3$
	0.92	216.0650	216.0655	-2.4	$C_{12}H_{10}NO_3$
EOMCC 246	1.55	89.0381	89.0386	-5.3	C_7H_5
MSMS 216	0.82	104.0490	104.0495	-4.6	C_7H_6N
ES+	0.34	105.0330	105.0335	-4.7	C_7H_5O
	12.55	116.0490	116.0495	-4.1	C_8H_6N
	7.50	132.0438	132.0444	-4.5	C_8H_6NO
	30.76	144.0438	144.0444	-4.1	C_9H_6NO
	4.53	160.0387	160.0393	-3.8	$C_9H_6NO_2$
	4.24	162.0544	162.0550	-3.4	$C_9H_8NO_2$
	100.00	188.0336	188.0342	-3.3	$C_{10}H_6NO_3$
	2.49	216.0649	216.0655	-2.9	$C_{12}H_{10}NO_3$

Table 2.2. Exact mass and formula predictions for the MS/MS data in Figure 2.5.

Appendix 2.2 Measured Rates and Selectivities

Buffer Type	pH	Buffer Concentration (mM)	Temperature (°C)	$-r_{NADPH}$	$-r_{EOMCC}$	r_{7HCC}	Coupling $(-r_{EOMCC}) / (-r_{NADPH})$	Regioselectivity $(r_{7HCC}) / (-r_{EOMCC})$
KPi	6.2	100	25	41.4 ± 6.1	2.9 ± 0.2	0.53 ± 0.02	6.9 ± 1.1 %	18.6 ± 1.2 %
KPi	6.7	100	25	77.8 ± 7.3	6.1 ± 0.5	1.37 ± 0.04	7.9 ± 1.0 %	22.4 ± 2.0 %
KPi	7.2	100	25	55.3 ± 18.0	5.9 ± 0.6	1.68 ± 0.04	10.7 ± 3.7 %	28.4 ± 3.1 %
KPi	7.7	100	25	48.7 ± 7.6	5.6 ± 0.1	1.74 ± 0.05	11.6 ± 1.8 %	30.9 ± 1.1 %
KPi	8.2	100	25	23.9 ± 8.1	5.1 ± 0.9	0.53 ± 0.01	21.3 ± 8.1 %	10.4 ± 1.8 %
Tris	7.1	100	25	43.7 ± 6.4	5.9 ± 0.9	1.25 ± 0.07	13.4 ± 2.8 %	21.4 ± 3.5 %
Tris	7.6	100	25	33.5 ± 4.0	5.9 ± 0.5	0.67 ± 0.04	17.5 ± 2.6 %	11.4 ± 1.2 %
Tris	8.1	100	25	36.7 ± 7.9	4.0 ± 0.4	0.40 ± 0.01	10.9 ± 2.6 %	10.0 ± 1.1 %
Tris	8.6	100	25	24.8 ± 7.6	2.4 ± 0.6	0.22 ± 0.02	9.8 ± 3.8 %	9.2 ± 2.4 %
Tris	9.1	100	25	n.d.	n.d.	0.11 ± 0.03	n.d.	n.d.
KPi	6.7	15	25	47.9 ± 16.7	3.6 ± 0.3	0.60 ± 0.01	7.4 ± 2.7 %	17.0 ± 1.6 %
KPi	6.7	50	25	56.9 ± 7.2	3.4 ± 0.2	0.86 ± 0.02	5.9 ± 0.9 %	25.7 ± 2.2 %
KPi	6.7	100	25	77.8 ± 7.3	6.1 ± 0.5	1.37 ± 0.04	7.9 ± 1.0 %	22.4 ± 2.0 %
KPi	6.7	150	25	108.2 ± 32.1	8.3 ± 0.6	1.85 ± 0.05	7.7 ± 2.3 %	22.3 ± 1.6 %
KPi	6.7	250	25	125.7 ± 12.5	11.0 ± 1.1	2.58 ± 0.25	8.7 ± 1.2 %	23.5 ± 3.2 %
KPi	6.7	375	25	136.6 ± 14.2	13.1 ± 0.5	2.51 ± 0.05	9.6 ± 1.0 %	19.2 ± 0.8 %
KPi	6.7	675	25	111.6 ± 13.0	7.9 ± 0.8	2.05 ± 0.05	7.1 ± 1.1 %	26.1 ± 2.8 %
KPi	6.7	250	25	125.7 ± 12.5	11.0 ± 1.1	2.58 ± 0.25	8.7 ± 1.2 %	23.5 ± 3.2 %
KPi	6.7	250	29	169.5 ± 15.4	11.5 ± 0.7	2.78 ± 0.06	6.8 ± 0.7 %	24.1 ± 1.6 %
KPi	6.7	250	33	188.5 ± 14.3	15.8 ± 0.4	3.23 ± 0.13	8.4 ± 0.7 %	20.4 ± 1.0 %
KPi	6.7	250	37	227.4 ± 16.5	18.4 ± 0.4	3.81 ± 0.13	8.1 ± 0.6 %	20.6 ± 0.8 %
KPi	6.7	250	41	270.8 ± 26.0	21.8 ± 1.2	4.45 ± 0.15	8.0 ± 0.9 %	20.4 ± 1.3 %
KPi	6.7	250	45	284.7 ± 30.1	20.3 ± 1.2	4.67 ± 0.20	7.1 ± 0.9 %	23.0 ± 1.7 %

Table 2.3. Measured rates and selectivities of the CYP1A2 oxidation of EOMCC under different reaction conditions

CHAPTER 3

Specific and General Ion Effects on P450 Catalysis

3.1 Abstract

Although the large effect of ion type and concentration on cytochrome P450 catalysis is well documented, the full kinetic consequence of this effect has yet to be explored. We measured the CYP1A2 and CYP3A4 mediated O-dealkylation of alkoxycoumarins as a function of ion type and concentration for twelve salts. We found that greatest rate enhancement for both isoforms with potassium fluoride, yielding increases of 19 and 2.5 fold for CYP3A4 and CYP1A2, respectively. Moreover, we measured the kinetic parameters and noncompetitive intermolecular isotope effect for the O-dealkylation of 7-methoxy-3-cyanocoumarin by CYP1A2 as a function of potassium fluoride and P450-reductase content. We found the rate increases seen with potassium fluoride were primarily due to increases in k_{cat}. Furthermore, the noncompetitive intermolecular isotope effect was large (~6) and constant for all conditions assayed. A simplified P450 mechanism was used to support the possibility that the large isotope effects seen in this and other P450 systems is due primarily to the large rate of uncoupling, which serves to unmask the intrinsic isotope effect.

3.2 Introduction

Cytochrome P450 enzymes are a diverse family of monooxygenases present in all types of life (*1*). P450 catalysis occurs at the iron center of a heme cofactor where two electrons, sequentially supplied by cytochrome P450 reductase, activate molecular dioxygen to form a highly reactive iron-oxo species (*2*). This reactive species can perform a wide variety of oxidative transformations to accomplish the varied biological roles of these enzymes (*3*). The diversity and specificity of chemical transformations catalyzed by P450 enzymes, often on unreactive carbon centers, have made them attractive catalysts from a synthetic perspective (*4*). Human drug-metabolizing P450 enzymes, as the primary route of first-pass metabolism of exogenous compounds, are particularly attractive due to their evolved substrate promiscuity (*5*). However, the low rates characteristic of these enzymes have rendered them currently impractical (*6*). Simple variations in reaction conditions are known to increase P450 reaction rates by orders of magnitude. In particular, P450 catalysis is affected by the nature and concentration of ionic species present in the reaction medium (*7-10*), but the kinetic implications of this effect are poorly understood.

In general, P450 reaction rates exhibit an optimum in rate as buffer concentration, a proxy for ionic strength, is varied (*9*). In particular, however, different buffer salts can yield diverse results. CYP3A4 testosterone 6β-hydroxylation was stimulated 3-fold by a change from potassium phosphate to potassium HEPES buffer at the same concentration (*8*). Additionally, divalent cations increased CYP3A4 mediated nifedipine oxidation by 2-fold, while the inclusion of monovalent cations yielded only marginal increases (*10*). Furthermore, the CYP1A2 mediated dealkylation of a substituted alkoxycoumarin exhibited a 3-fold difference in rate in phosphate versus HEPES buffers (chapter 2).

The study of ion effects on enzyme behavior often correlates with the Hofmeister ion series and is ascribed to the structure-making or structure-breaking character of

specific ions with water (*11*). This strength is quantified in the Jones-Dole B coefficient, an empirical parameter describing the change in viscosity of a solution with ion content (*12*). Nitric oxide synthases, which have structural and mechanistic similarities to P450 enzymes, exhibit ion specific salt effects, both activation and inhibition, that correlate with the Hofmeister series (*13, 14*). To the best of our knowledge, no studies have investigated the effect of a series of ions on P450 activity.

The origin of the effect of ions on P450 catalysis has been previously attributed to a modulation of the P450-reductase interaction (*15*), which has been shown to be mediated by ionic interactions. Positively charged amino acids on the proximal face of the P450 interact with negatively charged residues on the reductase, and this interaction is affected by changes in salt content. This model explains the observable optimum in activity with ion content. At low salt concentrations the P450 interacts too strongly with the reductase, while at high salt the interaction is not strong enough (*16*).

Kinetic isotope effects have been used to probe the catalysis of P450 enzymes for several decades. They have been useful in elucidating the kinetic mechanism, probing enzyme-substrate binding interactions, and relative active site size of P450 enzymes (*17*). Noncompetitive intermolecular isotope effects are measured by comparing the ratio of rates when the enzyme is incubated with a protiated versus a deuterated substrate. This value provides a measure of how rate limiting the C-H bond breaking step is in the overall mechanism (*17*). In general, mammalian P450 enzymes exhibit large noncompetitive intermolecular isotope effects (*18-22*).

This study has two goals. First, to quantify the differential effect of various ions on P450 catalysis and, second, to investigate the source of these effects with the hope of clarifying the conflicting conclusions that human drug-metabolizing P450 enzymes are simultaneously significantly rate-limited by the C-H bond breaking step and by the electron supply from the reductase. The former is observed in the large kinetic isotope effects measured in these systems and the later is evidenced by the attribution of ion effects on reaction rates to an alteration of the P450-reductase binding.

In this work, we used the CYP1A2 and CYP3A4 mediated O-dealkylation of alkoxycoumarins as a model system to investigate the effect of varying the concentration and identity of ions in the reaction medium. We found both activation and inhibition of product generation by different salts but no correlation with the Hofmeister series. In general, varying the anion yielded the greatest variations in rate, and the presence of KF gave the largest increase in rates for both isoforms. In addition, we measured the kinetic constants and noncompetitive intermolecular kinetic isotope effect in the O-demethylation of 7-methoxy-3-cyanocoumarin by CYP1A2 as a function of KF and reductase content. We found that the kinetic consequence of a variation in KF concentration was primarily exhibited in k_{cat} rather than K_M. Furthermore, we found that the noncompetitive intermolecular isotope effect was large and essentially constant for all studied KF concentrations and for systems with high and low concentrations of P450 reductase. Using a simplified model, we show that the large isotope effects observed in this study can be adequately explained by the unmasking effects of alternate pathways in the catalytic mechanism, such that no single step is rate-limiting but, rather, several steps contribute to the observed rate of O-demethylation.

3.3 Materials and Methods

3.3.1 Materials

Glucose-6-phosphate, glucose-6-phosphate dehydrogenase, nicotinamide adenine dinucleotide phosphate (NADP+), 2,4-dihydroxy-benzaldehyde, malonitrile, and both protiated and deuterated methyl iodide were purchased from Sigma (St. Louis, MO). Microsomes from baculovirus-infected insect cells (Baculosomes) expressing human P450 enzymes and rabbit cytochrome P450 reductase, 7-ethoxymethoxy-3-cyanocoumarin (EOMCC), and 7-benzyloxymethoxy-3-cyanocoumarin (BOMCC) were purchased from Invitrogen (Carlsbad, Ca). CYP1A2 Baculosomes were from lot 484429F, while CYP3A4 Baculosomes were from lot 539756F. Microsomes from *Escherichia coli* expressing human CYP1A2 and human P450-reductase (Bactosomes) were purchased from Xenotech (Lenexa, KS). Bactosomes were purchased with higher and lower reductase levels (Batch numbers C1A2R007/E and C1A2LR009/A). Calculating the reductase content of the Bactosomes with the method of Davydov et. al. (*23*) yields a CPR:P450 ratio of 1:5 and of 1:33 for the higher and lower-reductase systems, respectively. All chemicals were used as received. All fluorescence data were acquired on a Spectramax M2 plate reader (Molecular Devices, Sunnyvale, CA).

3.3.2 Synthesis of MCC and dMCC

The synthesis of protiated 7-methyl-3-cyanocoumarin (MCC) and the deuterated analog 7-[$^{2}H_3$]methyl-3-cyanocoumarin (dMCC) was conducted in three steps (Fig 3.1). The first two steps were conducted as described before (*24*). Briefly, 1.38 g of 2,4-dihydroxy-benzaldehyde (10 mmol) and 1.64 g malonitrile (12.5 mmol) were vigorously stirred in 100 mL of 50 mM $NaHCO_3$ for 1.5 hr in a round bottom flask equipped with a reflux condenser. 2.5 mL of 12 N HCl was added and the mixture was further stirred for 1 hr in a 90 °C oil bath. The final mixture was vacuum filtered and washed with 50 mL 0.1 N HCl to obtain 7-hydroxy-3-cyanocoumarin (HCC).

1.0 g HCC (5.34 mmol) was added to 1.0 g K_2CO_3 (7.24 mmol) in 100 ml acetone. The reaction was initiated with the addition of 661 µL of methyl iodide (10.6 mmol) and the mixture was stirred under reflux for 7 hr. Deuterated methyl iodide was used to generate dMCC. After 7 hr, the mixture was vacuum filtered and the filtrate was concentrated under vacuum. The resulting solid was dissolved in chloroform, washed three times with $NaHCO_3$ brine, dried with Na_2SO_4, filtered, then rotavapped to dryness. The resulting solid was recrystallized twice with ethyl acetate.

Characterization with NMR and mass spectrometry confirmed compound identity and purity. The mass spectra of purified MCC and dMCC (Fig 3.3) conform to the fragmentation pattern shown in Figure 3.2, where ions expected to contain a deuterated methyl group exhibit a larger mass by 3 amu. The NMR spectra in Figure 3.3 also indicate the successful incorporation of deuterium labels in the 7-methoxy group.

3.3.3 Activity Assays

All assays were conducted in duplicate at 25 °C in 25 mM potassium phosphate buffer at pH 7.4. The EOMCC and BOMCC dealkylation assays were conducted with 5 nM CYP1A2 and CYP3A4 Baculosomes, respectively. An NADPH regeneration system was included with 1 U/mL glucose-6-phosphate dehydrogenase and 3.3 mM glucose-6-

phosphate. Reactions were initiated with the simultaneous addition of 200 μM NADP+ and 5 μM substrate and monitored at an excitation and emission wavelength of 409 nm and 460 nm, respectively. Fluorescent standard curves were generated at each concentration of each salt tested to account for the variation in product fluorescence with ion content. The O-demethylation of MCC and dMCC was assayed with 10 nM of high and low reductase CYP1A2 Bactosomes under the same conditions.

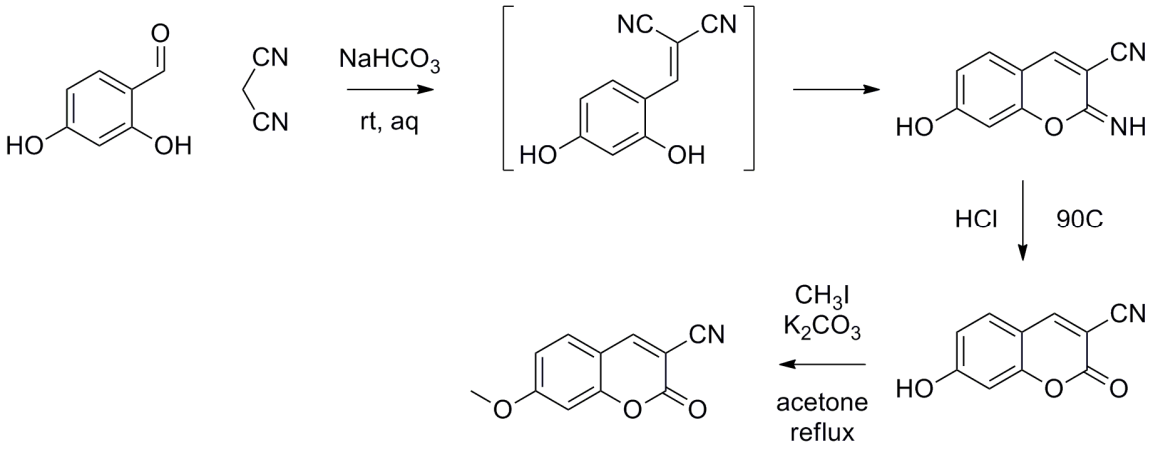

Figure 3.1. Synthesis of 7-methyl-3-cyanocoumarin substrates

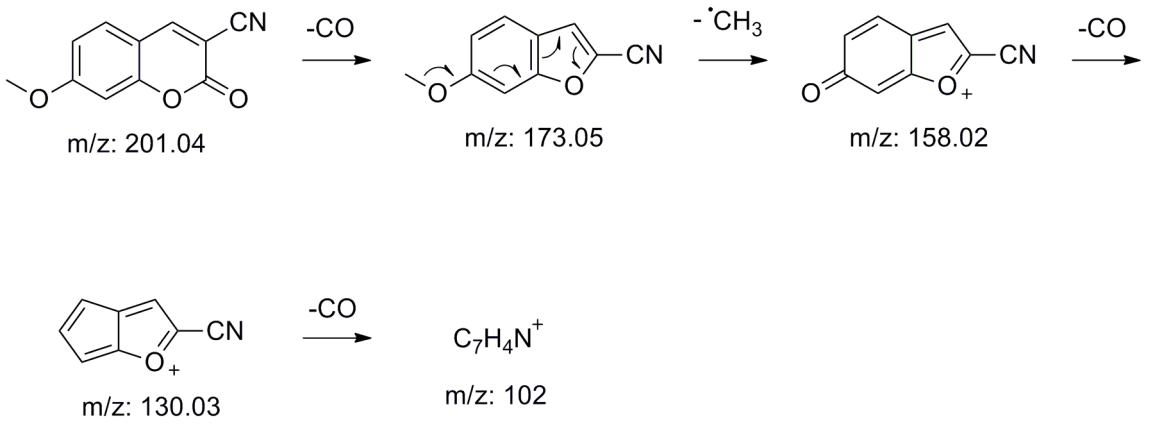

Figure 3.2. Proposed fragmentation pattern of MCC and dMCC

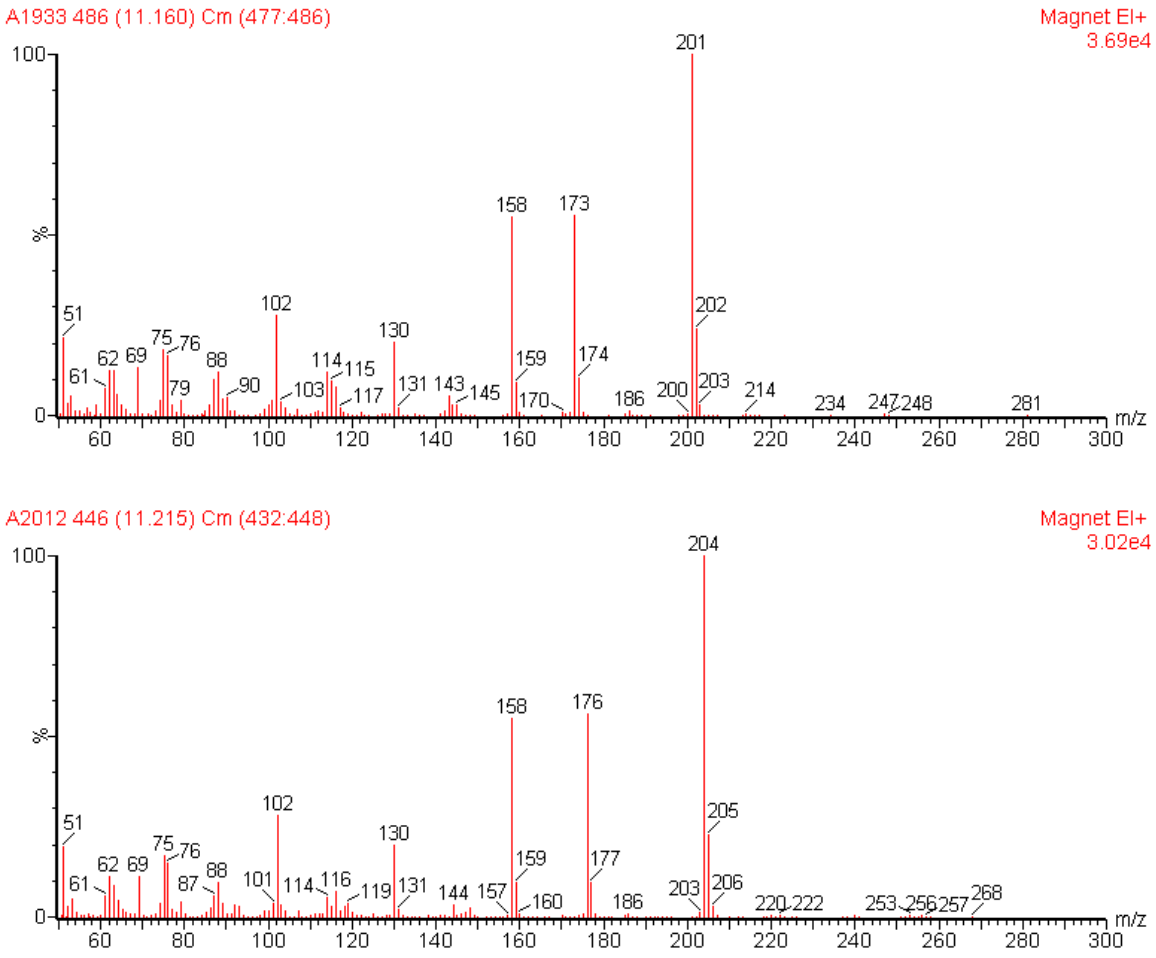

Figure 3.2. Electron impact mass spectrum of (top) MCC and (bottom) dMCC.

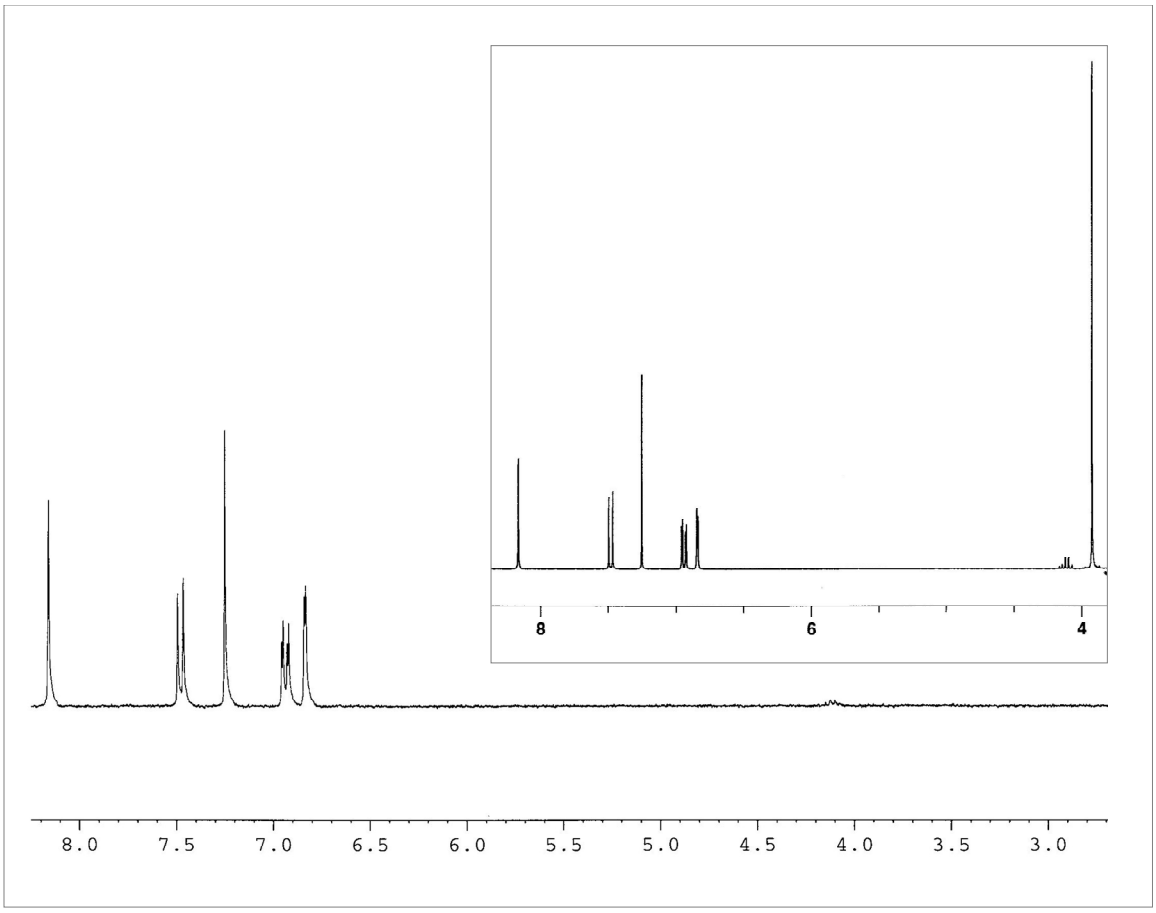

Figure 3.3. NMR spectra of (inset) MCC and dMCC

3.4 Results

3.4.1 Effect of Ions on CYP1A2 and CYP3A4 Activity

To characterize the scope and generality of P450 response to multiple types of ions, the O-dealkylation of EOMCC by CYP1A2 and of BOMCC by CYP3A4 to generate HCC was assayed in the presence of 12 salts (Fig 3.4, 3.5). With the exception of $MgCl_2$ on CYP1A2 and potassium formate on CYP3A4, all data exhibited an initial increase then decrease in P450 activity with salt content. In general, CYP3A4 activity exhibited the largest variations, with the identity of the anion having the greatest effect. Despite the previous literature heuristic that CYP3A4 catalysis is significantly promoted by magnesium (*9*), neither CYP3A4 nor CYP1A2 exhibited considerably increased rates in the presence of $MgCl_2$. Instead, fluoride salts increased reaction rates the most. Larger rate increases were observed as the cation moved up the periodic table, with the largest rates observed in the presence of KF, which increased the rate of CYP3A4 and CYP1A2 catalysis by 19 and 2.5 fold, respectively. NaF could not be assayed at high enough concentrations to observe an optimum due to solubility limits. No observable trend was identified with the Jones-Dole B coefficient of the ions (Table 3.1). Additionally, no activity was observed in the presence of the irreversible P450 inhibitor piperonyl butoxide, indicating that the origin of the salt affect lies in an interaction with the P450 (data not shown).

Anion	B	Cation	B
Formate	-0.052	Cs^+	-0.047
Cl^-	-0.05	Rb^+	-0.033
NO_3^-	-0.045	K^+	-0.009
F^-	0.127	Na^+	0.085
Acetate	0.246	Mg^{2+}	0.385

Table 3.1. Jones-Dole B coefficients of ions used in this study (*25*)

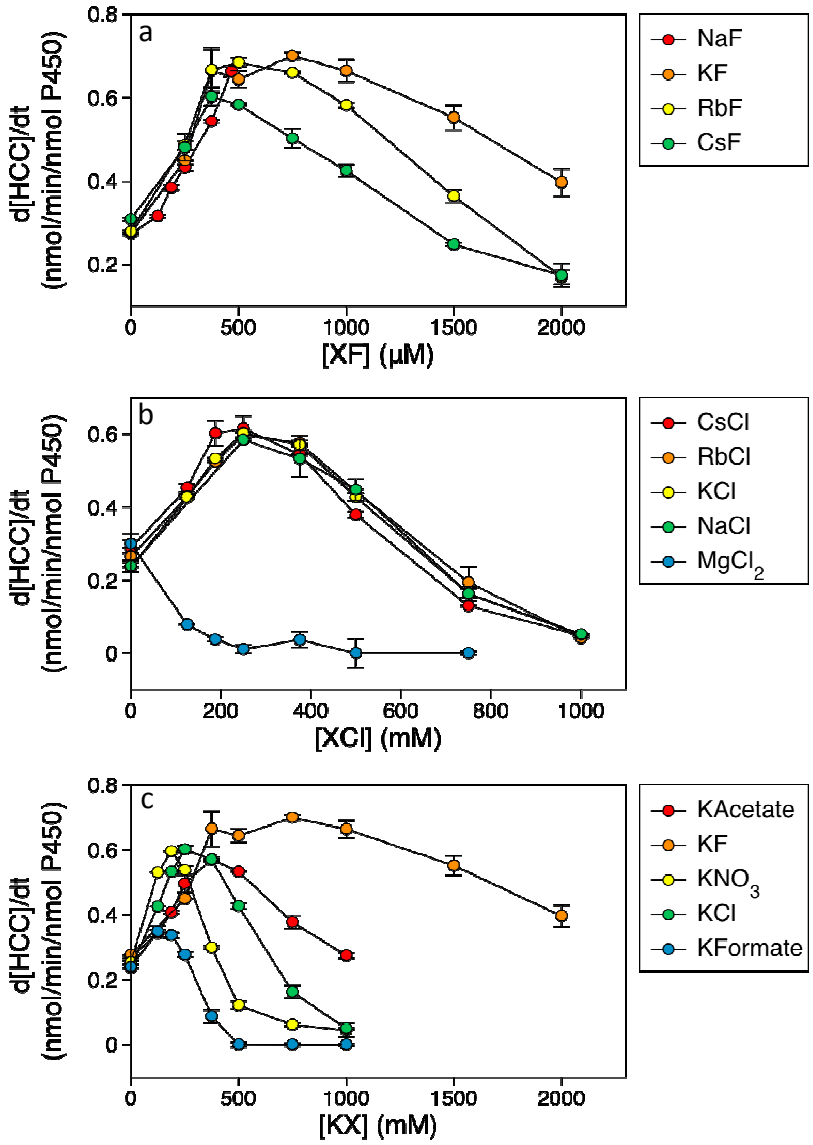

Figure 3.4. Variation of CYP1A2 dealkylation of EOMCC by (a) fluoride salts, (b) chloride salts, and (c) potassium salts. The legend is colored to correlate color with Jones-Dole B coefficient (i.e. red is the largest while blue is the lowest).

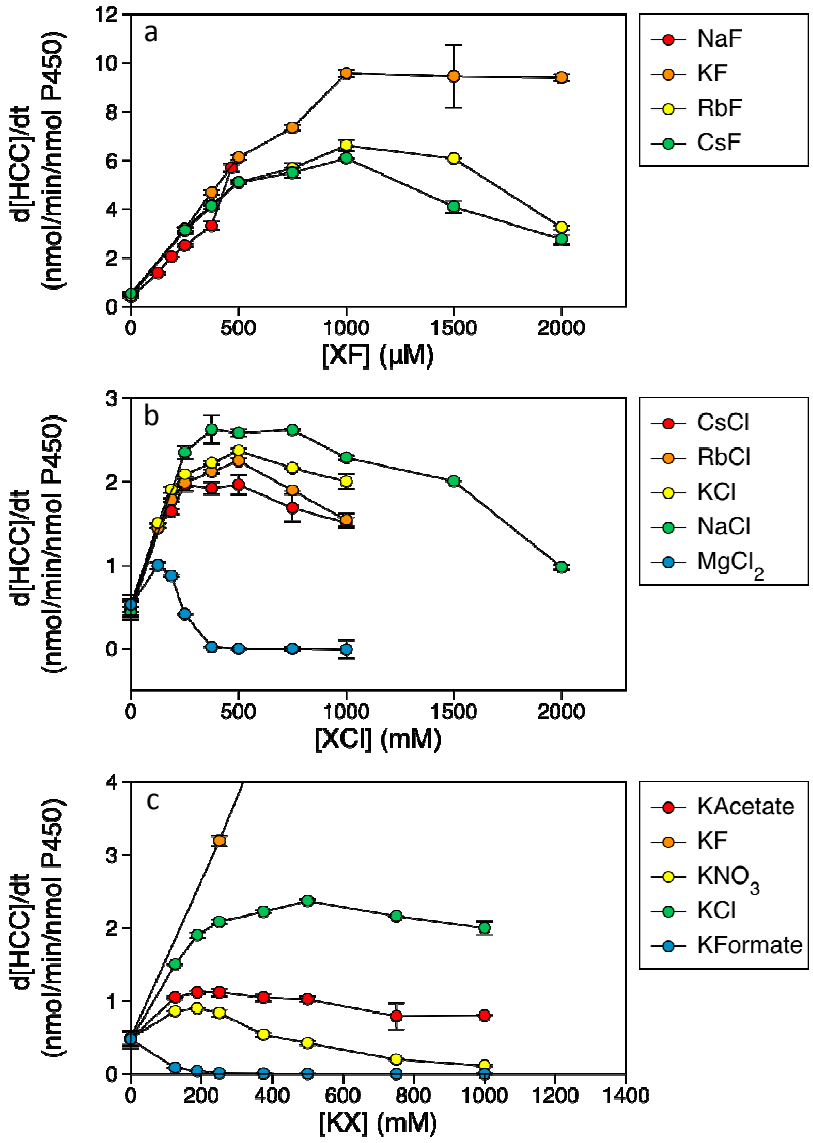

Figure 3.5. Variation of CYP3A4 dealkylation of BOMCC by (a) fluoride salts, (b) chloride salts, and (c) potassium salts. The legend is colored to correlate color with Jones-Dole B coefficient (i.e. red is the largest while blue is the lowest).

3.4.2 Kinetic Isotope Effects in CYP1A2 Catalysis

The effect of KF and reductase content on CYP1A2 catalysis was assessed in the O-demethylation of MCC and dMCC. Substrate-velocity curves were measured for 6 KF concentrations and 2 levels of reductase at a constant P450 content. Noncompetitive intermolecular isotope effects were calculated at all conditions. The O-demethylation of MCC and dMCC by CYP1A2 fit well to the Michaelis-Menten equation and yielded the kinetic constants shown in Figures 3.8 - 3.10. An optimum in k_{cat} was observed between 600 and 800 mM KF with both MCC and dMCC for both high and low reductase systems, which varied by roughly an order of magnitude in the high reductase system versus low reductase. The Michaelis constant, K_M, varied little with KF or with reductase

content, except with an increase at 200 mM KF in the low reductase system. Surprisingly, the noncompetitive intermolecular isotope effects on k_{cat} and k_{cat}/K_M, calculated as ${}^{H}k_{cat}$ / ${}^{D}k_{cat}$ and ${}^{H}(k_{cat}/K_M)$ / ${}^{D}(k_{cat}/K_M)$, respectively, were effectively constant as both KF and reductase were varied.

$$E + S \underset{k_{21}}{\overset{k_{12}}{\rightleftharpoons}} ES \underset{k_{32}}{\overset{k_{23}}{\rightleftharpoons}} ES^* \xrightarrow{k_{34}} E + P \tag{1}$$

$$k_{cat} = \frac{k_{23}k_{34}}{k_{23} + k_{32} + k_{34}} \tag{2}$$

$$K_M = \frac{k_{21}k_{32} + k_{21}k_{34} + k_{23}k_{34}}{k_{12}\left(k_{23} + k_{32} + k_{34}\right)} \tag{3}$$

$$\frac{{}^{H}k_{cat}}{{}^{D}k_{cat}} = \frac{k_{34H}/k_{34D} + \dfrac{k_{34H}/k_{23}}{k_{32}/k_{23} + 1}}{1 + \dfrac{k_{34H}/k_{23}}{k_{32}/k_{23} + 1}} \tag{4}$$

$$\frac{{}^{H}\left(k_{cat}/K_M\right)}{{}^{D}\left(k_{cat}/K_M\right)} = \frac{k_{34H}/k_{34D} + \dfrac{k_{34H}\left(1/k_{23} + 1/k_{21}\right)}{k_{32}/k_{23}}}{1 + \dfrac{k_{34H}\left(1/k_{23} + 1/k_{21}\right)}{k_{32}/k_{23}}} \tag{5}$$

A simplified P450 reaction mechanism is shown in Equation 1. This model, adapted from that of Korzekwa et al (*26*), encompasses several relevant characteristics of the P450 mechanism. Equation 1 contains an activation step where the enzyme-substrate complex, ES, is activated to ES*. This step includes both 1-electron reductions by the P450 reductase and the necessary rearrangements to generate the active iron-oxo species. Equation 1 also contains a reverse step where the activated complex, ES*, reverts to ES. This step includes all possible pathways by which the ES* complex does not generate fluorescent HCC product, including uncoupled pathways and the oxidation of alternate sites on the substrate. Equations describing the kinetic parameters and kinetic isotope effects derived from Equation 1 are shown in Equations 2 - 5. These equations were fit to the data measured in Figures 3.8 – 3.10 with the assumption that only k_{23} varied with KF or reductase content. All other parameters in Equations 2 – 5 were held constant for all conditions. The resulting fits are shown in Figures 3.8 – 3.10 and the fit parameters are in Tables 3.2 and 3.3. Except for the increase in K_M at 200 mM KF in the low reductase system, all major features of the data were captured in this simplified model.

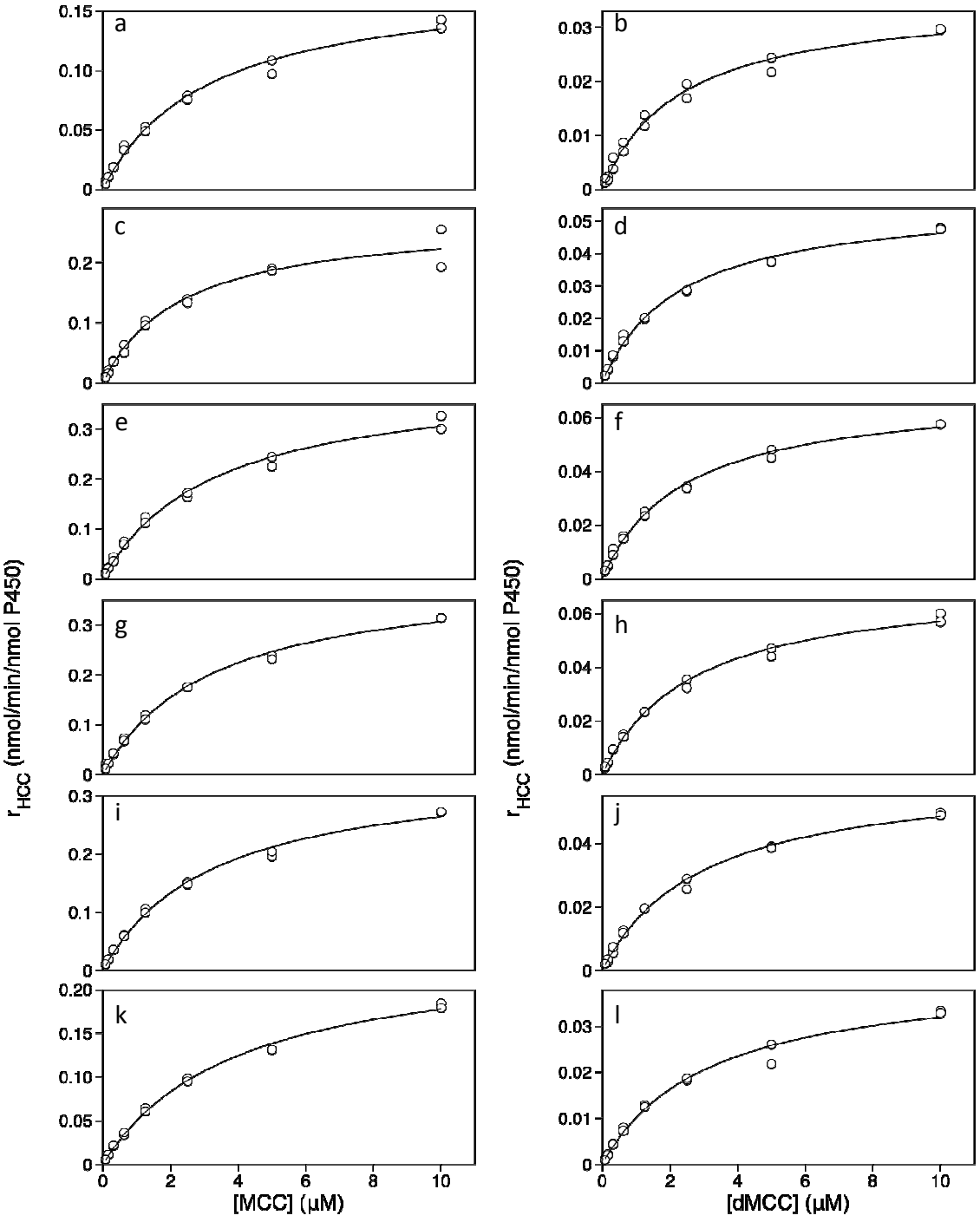

Figure 3.6. Velocity curves are plotted as a function of MCC and dMCC concentration for the high-reductase CYP1A2 system in the presence of (a, b) 1.6 M KF, (c, d) 1.2 M KF, (e, f) 0.8 M KF, (g, h) 0.6 M KF, (i, j) 0.4 M KF, (k, l) 0.2 M KF. Fits are to the Michaelis-Menten equation.

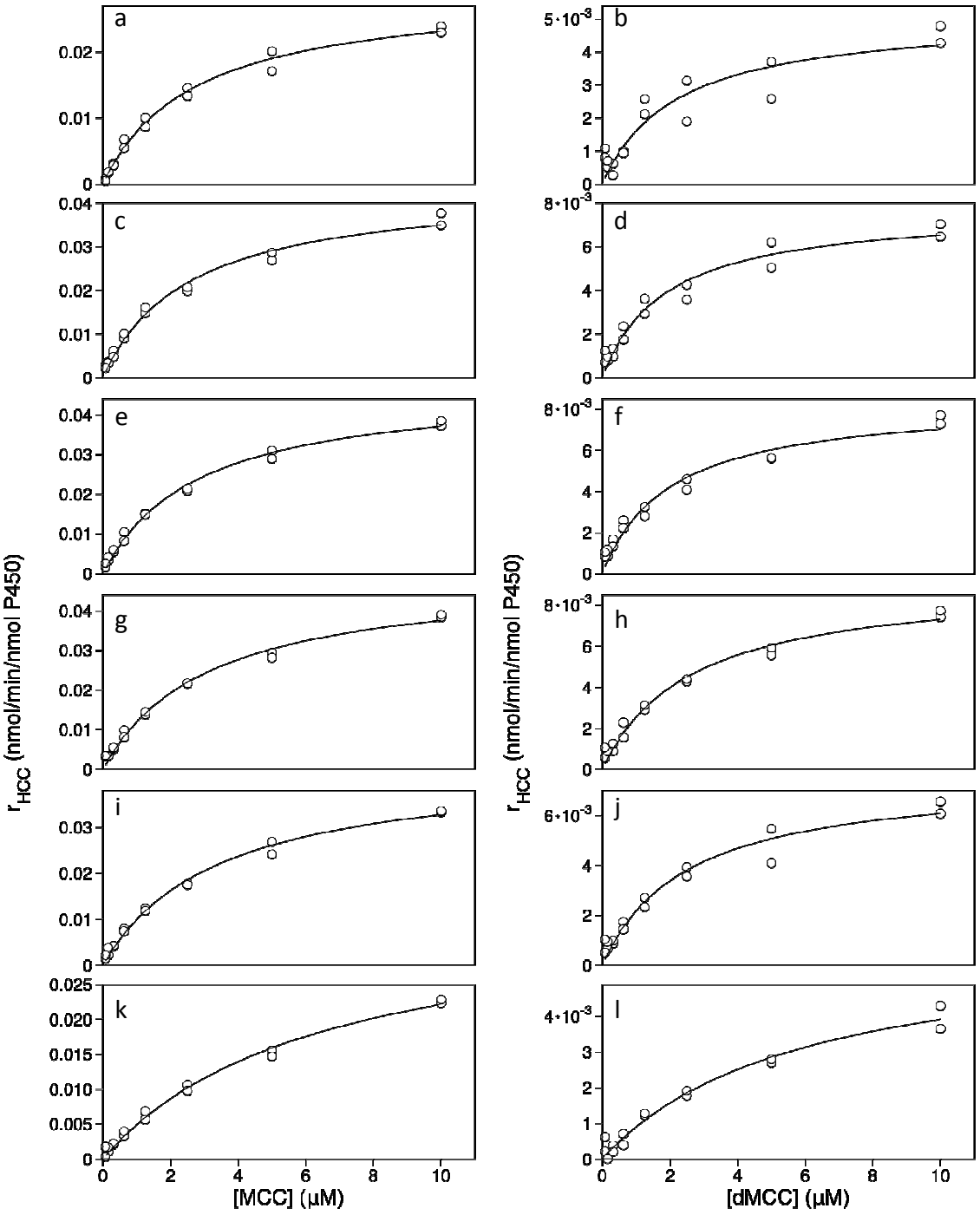

Figure 3.7. Velocity curves are plotted as a function of MCC and dMCC concentration for the low-reductase CYP1A2 system in the presence of (a, b) 1.6 M KF, (c, d) 1.2 M KF, (e, f) 0.8 M KF, (g, h) 0.6 M KF, (i, j) 0.4 M KF, (k, l) 0.2 M KF. Fits are to the Michaelis-Menten equation.

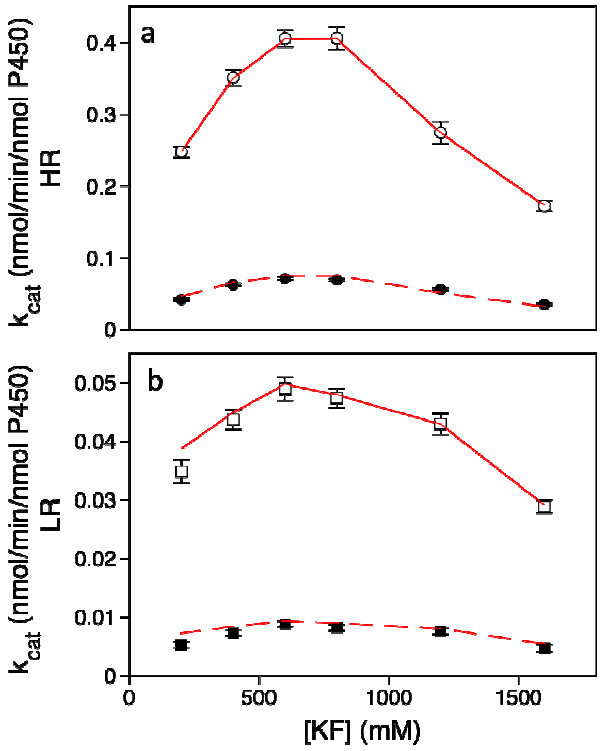

Figure 3.8. Calculated k_{cat} values for (a) the high-reductase and (b) the low-reductase CYP1A2 systems are plotted as a function of KF concentration. Open shapes denote data taken with the protiated, MCC substrate, while filled shapes denote data from the deuterated, dMCC substrate. The fit lines are plotted using the parameters in Table 3.2 and Table 3.3 in Equation 2 for (solid red) MCC and (dashed red) dMCC.

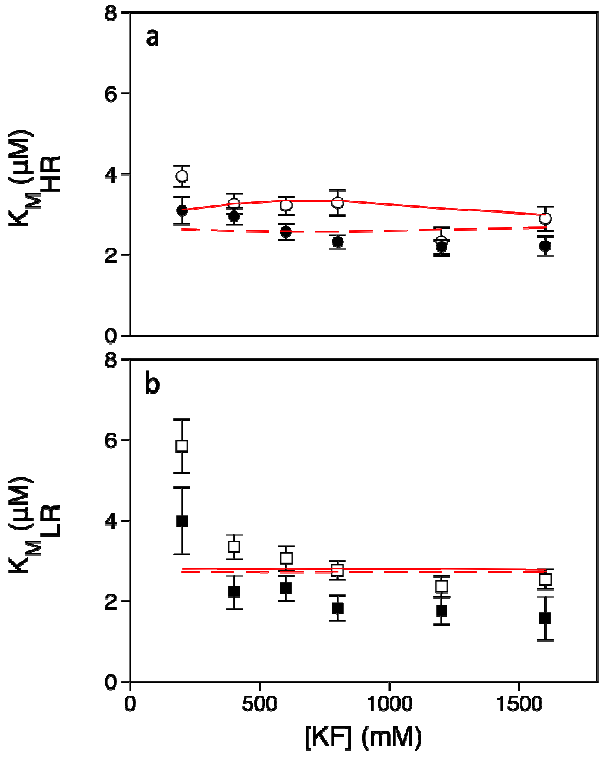

Figure 3.9. Calculated K_M values for (a) the high-reductase and (b) the low-reductase CYP1A2 systems are plotted as a function of KF concentration. Open shapes denote data taken with the protiated, MCC substrate, while filled shapes denote data from the deuterated, dMCC substrate. The fit lines are plotted using the parameters in Table 3.2 and Table 3.3 in Equation 3 for (solid red) MCC and (dashed red) dMCC.

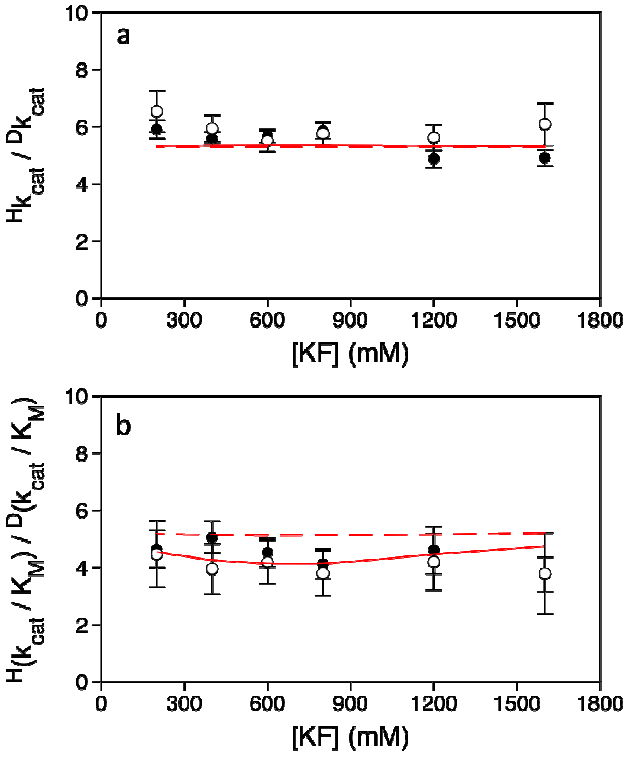

Figure 3.10. Noncompetitive intermolecular isotope effects for (open shapes) the high-reductase and (filled shapes) the low-reductase CYP1A2 systems are plotted as a function of KF concentration. The fit lines are plotted using the parameters in Table 3.2 and Table 3.3 in Equations 4 and 5 for (solid red) MCC and (dashed red) dMCC.

Rate constant	Value
k_{12}	0.44 $\mu M^{-1}min^{-1}$
k_{21}	1.22 min^{-1}
k_{32}	34.5 min^{-1}
k_{34H}	3.65 min^{-1}
k_{34D}	0.63 min^{-1}

Table 3.2. Rate constants used in fitting Equations 2 - 5 to the data in Figures 3.8 – 3.10.

[KF] (M)	High-Reductase k_{23} (min^{-1})	Low-Reductase k_{23} (min^{-1})
1.6	1.90	0.31
1.2	3.10	0.45
0.8	4.76	0.51
0.6	4.76	0.53
0.4	4.05	0.48
0.2	2.78	0.41

Table 3.2. Rate constants used in fitting Equations 2 - 5 to the data in Figures 3.8 – 3.10.

3.5 Discussion

3.5.1 Effect of Ions on CYP1A2 and CYP3A4 Catalysis

With the exception of $MgCl_2$ on CYP1A2 and potassium formate on CYP3A4, all data exhibited an initial increase then decrease in P450 activity with salt content. The salt concentration yielding optimal activity and the magnitude of this optimum varied with ion type more with CYP3A4 than with CYP1A2. This suggests that the response of CYP3A4 is governed more by specific ion effects while the response of CYP1A2 is governed more by general ion effects, such as ionic strength. Additionally, neither isoform exhibited responses that correlated with the Jones-Dole B coefficient. Since this coefficient describes an ion's interaction with water and correlates with protein hydration (*11*), these must not be relevant ion parameters in these systems.

3.5.2 Kinetic Isotope Effects in CYP1A2 Catalysis

Noncompetitive intermolecular isotope effects can provide unique insights into the mechanism of enzymatic reactions. The observed isotope effect is dependent on the intrinsic isotope effect, the ratio of the rates of the isotopically sensitive reaction step, and also on other rates in the overall mechanism. This leads to the general description of isotope effects as a measure of how rate-limiting the C-H bond breaking step is in the overall mechanism (*27*). If another, non-isotopically sensitive step is rate-limiting; the overall reaction rate is determined by the rate of that step, and the actual difference in rates of breaking a C-D bond versus a C-H bond, the intrinsic isotope effect, will be masked by the rate of the slower step.

Alternatively, if a reaction mechanism generates multiple products, the intrinsic isotope effect in the isotopically sensitive step will be unmasked (*26*). This is relevant for P450 enzymes which can oxidize a substrate at multiple locations and are also prone to uncoupling. The origin and consequence of masking can be more clearly seen in equations describing the enzymatic mechanism. The simplified model, shown in Equation 1, can be used to approximate a P450 system. All steps after substrate binding and before oxidation, including the two reduction steps and rearrangements necessary to generate the active iron-oxo species, are encompassed in the step with rate k_{23}. All possible pathways from an activated enzyme-substrate complex that don't lead to fluorescent product generation by O-demethylation are encompassed in the step with rate k_{32}. This includes the oxidation of other sites on the substrate and uncoupling pathways. The CYP1A2 oxdiation of coumarin substrates is known to be mostly uncoupled (~90%) and to produce several products resulting from attacking the substrate at alternate locations (chapter 2). It is clear from Equation 4 that if k_{23} is large, the intrinsic isotope effect will be masked and the measured value will be decreased, approaching a limiting value of 1. This situation could correspond to an increase in reductase content, where the donation of electrons to the P450, and thus k_{23}, would increase. It is also clear that as k_{32} increases in Equation 4, the intrinsic isotope effect would be unmasked and the measured value would increase, approaching the intrinsic value. Finally, the isotope effect on k_{cat}/K_M, shown in Equation 5, approaches the value of the isotope effect on k_{cat}, shown in Equation 4, as the value of k_{21} increases.

Equations 2 – 5 were fit to the data shown in Figures 3.8 – 3.10. Based on the assumption that a variation in the reductase or ion content of the reaction medium will

manifest only in an alteration of the P450-reductase interaction, all parameters except k_{23} were held constant over all of the conditions tested. Even with so many parameters held constant, this is not a unique solution. Rather, it is meant to illustrate that the type of rate variations acquired in these experiments are consistent with a model where KF and reductase content only affect k_{23} processes in the P450 mechanism. Furthermore, the high and effectively constant noncompetitive intermolecular isotope effects are due primarily to the large value of k_{32}. The high amount of uncoupling and alternate product generation previously observed in the CYP1A2 oxidation of coumarins (chapter 2) is also seen in this high value for k_{32}. The large flux through these non-isotopically sensitive pathways serves to unmask the intrinsic isotope effect, and the intrinsic value in this model of 5.8 is quite close to the measured and calculated values in Figure 3.10A.

A previous study investigated the catalysis of several human CYP1A2 mutants with catalytic activities spanning 800 fold (*22*). The authors measured the rates of experimentally accessible steps in the P450 mechanism for the mutants, including substrate binding, the first 1-electron reduction, O_2 binding, autooxidation of the resulting ferric-superoxo species, and product binding, and found no significant differences among the mutants to explain the large differences in activity. They also measured similar noncompetitive intermolecular kinetic isotope effects in the oxidation of phenacetin, which led them to conclude that, although the rate varies considerably among the mutants, the mechanism must remain similar to explain the constant kinetic isotope effects. This result is similar to the current result, where the measured P450 activity spans orders of magnitude as the salt and reductase content are varied, but the observed kinetic isotope effect is large and constant. Yun et al. also found the majority of reducing equivalents from NADPH were lost to uncoupled pathways. The large noncompetitive intermolecular isotope effects observed in the CYP1A2 oxidation of MCC in this study, of phenacetin in the work of Yun et al., and of several other CYP1A2 substrates (*18, 19*) could be due to the large proportion of reducing equivalents lost to uncoupled pathways and alternate oxidations at non-isotopically sensitive sites. Taken in the context of the model shown in Equation 1, these alternate pathways increase k_{32}, which will unmask the isotope effect (Equation 4). This line of reasoning could be extended to describe the large noncompetitive intermolecular isotope effects observed in human drug-metabolizing P450 systems in general, because multiple oxidation products and high uncoupling are hallmarks of these systems.

It is important to point out, however, that the current results can be interpreted in multiple ways. Alternatively, CYP1A2 could exist in two or more discrete homo-oligomeric states and the effect of KF and reductase variations could be primarily due to an alteration in the ratio of different CYP1A2 states such that the amount of catalyst rather than specific catalytic steps are altered. Ion effects have been implicated in altering the heteromeric oligomerization of P450 enzymes (*28, 29*). While the existence and functional relevance of homomeric complexes formed by CYP1A2 (*30*) and CYP3A4 (*31-33*) have been established, the effect of ions on this interaction has yet to be investigated. It seems unlikely, however, that the active-site mutants studied by Yun et. al. could be affecting the oligomerization state.

In conclusion, CYP1A2 and CYP3A4 mediated O-dealkylation of alkoxycoumarins was assayed as function of twelve salt concentrations. Potassium fluoride yielded the highest rates in both systems, while neither isoform exhibited a

response that correlated with the Hofmeister series. The kinetic parameters and noncompetitive intermolecular isotope effect of the O-demethylation of MCC by CYP1A2 was measured as a function of KF and reductase concentration. The majority of the rate variation due to either parameter was manifested in k_{cat} rather than K_M. The kinetic isotope effects measured were between 5 – 6 and effectively constant over all experiments. A simplified model was used to support the thesis that the large isotope effects observed in mammalian P450 enzymes are due to the unmasking effects of the high rates of alternate non-isotopically sensitive pathways, such as uncoupling or other potential oxidation products.

3.6 References

1. Ortiz de Montellano, P. R. (2005) *Cytochrome P450: Structure, Mechansim, and Biochemistry*, 3rd ed. ed., Plenum Press, New York.
2. Denisov, I. G., Makris, T. M., Sligar, S. G., and Schlichting, I. (2005) Structure and chemistry of cytochrome P450, *Chem Rev 105*, 2253-2277.
3. Guengerich, F. P. (2001) Common and uncommon cytochrome P450 reactions related to metabolism and chemical toxicity, *Chem Res Toxicol 14*, 611-650.
4. Julsing, M. K., Cornelissen, S., Buhler, B., and Schmid, A. (2008) Heme-iron oxygenases: powerful industrial biocatalysts?, *Current Opinion in Chemical Biology 12*, 177-186.
5. Gillam, E. M. J. (2007) Extending the capabilities of nature's most versatile catalysts: Directed evolution of mammalian xenobiotic-metabolizing P450s, *Archives of Biochemistry and Biophysics 464*, 176-186.
6. Urlacher, V. B., Lutz-Wahl, S., and Schmid, R. D. (2004) Microbial P450 enzymes in biotechnology, *Appl Microbiol Biot 64*, 317-325.
7. Schenkman, J. B., Voznesensky, A. I., and Jansson, I. (1994) Influence of Ionic-Strength on the P450 Monooxygenase Reaction and Role of Cytochrome B(5) in the Process, *Archives of Biochemistry and Biophysics 314*, 234-241.
8. Yamazaki, H., Gillam, E. M. J., Dong, M. S., Johnson, W. W., Guengerich, F. P., and Shimada, T. (1997) Reconstitution of recombinant cytochrome P450 2C10(2C9) and comparison with cytochrome P450 3A4 and other forms: Effects of cytochrome P450-P450 and cytochrome P450-b(5) interactions, *Archives of Biochemistry and Biophysics 342*, 329-337.
9. Yamazaki, H., and Shimada, T. (2006) Cytochrome P450 reconstitution systems, *Methods Mol Biol 320*, 61-71.
10. Yamazaki, H., Ueng, Y. F., Shimada, T., and Guengerich, F. P. (1995) Roles of Divalent Metal-Ions in Oxidations Catalyzed by Recombinant Cytochrome-P450 3a4 and Replacement of Nadph-Cytochrome P450 Reductase with Other Flavoproteins, Ferredoxin, and Oxygen Surrogates, *Biochemistry-Us 34*, 8380-8389.
11. Bauduin, P., Renoncourt, A., Touraud, D., Kunz, W., and Ninham, B. W. (2004) Hofmeister effect on enzymatic catalysis and colloidal structures, *Curr Opin Colloid In 9*, 43-47.
12. Jenkins, H. D. B., and Marcus, Y. (1995) Viscosity B-coefficients of ions in solution, *Chem Rev 95*, 2695-2724.

13. Nishimura, J. S., Narayanasami, R., Miller, R. T., Roman, L. J., Panda, S., and Masters, B. S. S. (1999) The stimulatory effects of Hofmeister ions on the activities of neuronal nitric-oxide synthase - Apparent substrate inhibition by L-arginine is overcome in the presence of protein-destabilizing agents, *J Biol Chem 274*, 5399-5406.
14. Schrammel, A., Gorren, A. C. F., Stuehr, D. J., Schmidt, K., and Mayer, B. (1998) Isoform-specific effects of salts on nitric oxide synthase activity, *Bba-Protein Struct M 1387*, 257-263.
15. Davydov, D. R., Kariakin, A. A., Petushkova, N. A., and Peterson, J. A. (2000) Association of cytochromes P450 with their reductases: Opposite sign of the electrostatic interactions in P450BM-3 as compared with the microsomal 2B4 system, *Biochemistry-Us 39*, 6489-6497.
16. Voznesensky, A. I., and Schenkman, J. B. (1994) Quantitative-Analyses of Electrostatic Interactions between Nadph-Cytochrome P450 Reductase and Cytochrome-P450 Enzymes, *J Biol Chem 269*, 15724-15731.
17. Nelson, S. D., and Trager, W. F. (2003) The use of deuterium isotope effects to probe the active site properties, mechanism of cytochrome P450-catalyzed reactions, and mechanisms of metabolically dependent toxicity, *Drug Metab Dispos 31*, 1481-1498.
18. Guengerich, F. P., Krauser, J. A., and Johnson, W. W. (2004) Rate-limiting steps in oxidations catalyzed by rabbit cytochrome P450 1A2, *Biochemistry-Us 43*, 10775-10788.
19. Kim, K. H., Isin, E. M., Yun, C. H., Kim, D. H., and Guengerich, F. P. (2006) Kinetic deuterium isotope effects for 7-alkoxycoumarin O-dealkylation reactions catalyzed by human cytochromes P450 and in liver microsomes - Rate-limiting C-H bond breaking in cytochrome P450 1A2 substrate oxidation, *Febs J 273*, 2223-2231.
20. Krauser, J. A., and Guengerich, F. P. (2005) Cytochrome P450 3A4-catalyzed testosterone 6 beta-hydroxylation stereochemistry, kinetic deuterium isotope effects, and rate-limiting steps, *J Biol Chem 280*, 19496-19506.
21. Yun, C. H., Kim, K. H., Calcutt, M. W., and Guengerich, F. P. (2005) Kinetic analysis of oxidation of coumarins by human cytochrome P450 2A6, *J Biol Chem 280*, 12279-12291.
22. Yun, C. H., Miller, G. P., and Guengerich, F. P. (2000) Rate-determining steps in phenacetin oxidations by human cytochrome P450 1A2 and selected mutants, *Biochemistry-Us 39*, 11319-11329.
23. Davydov, D. R., Davydova, N. Y., Tsalkova, T. N., and Halpert, J. R. (2008) Effect of glutathione on homo- and heterotropic cooperativity in cytochrome P450 3A4, *Archives of Biochemistry and Biophysics 471*, 134-145.
24. Fringuelli, F., Piermatti, O., and Pizzo, F. (2003) One-pot synthesis of 3-carboxycoumarins via consecutive knoevenagel and pinner reactions in water, *Synthesis-Stuttgart*, 2331-2334.
25. Marcus, Y. (1997) *Ion properties*, Marcel Dekker, New York.
26. Korzekwa, K. R., Trager, W. F., and Gillette, J. R. (1989) Theory for the Observed Isotope Effects from Enzymatic Systems That Form Multiple Products

Via Branched Reaction Pathways - Cytochrome-P-450, *Biochemistry-Us 28*, 9012-9018.
27. Northrop, D. B. (1982) Deuterium and Tritium Kinetic Isotope Effects on Initial Rates, *Method Enzymol 87*, 607-625.
28. Kelley, R. W., Cheng, D. M., and Backes, W. L. (2006) Heteromeric complex formation between CYP2E1 and CYP1A2: Evidence for the involvement of electrostatic interactions, *Biochemistry-Us 45*, 15807-15816.
29. Kelley, R. W., Reed, J. R., and Backes, W. L. (2005) Effects of ionic strength on the functional interactions between CYP2134 and CYP1A2, *Biochemistry-Us 44*, 2632-2641.
30. Reed, J. R., Eyer, M., and Backes, W. L. (2010) Functional Interactions between Cytochromes P450 1A2 and 2B4 Require Both Enzymes to Reside in the Same Phospholipid Vesicle EVIDENCE FOR PHYSICAL COMPLEX FORMATION, *J Biol Chem 285*, 8942-8952.
31. Davydov, D. R., Fernando, H., Baas, B. J., Sligar, S. G., and Halpert, J. R. (2005) Kinetics of dithionite-dependent reduction of cytochrome P450 3A4: Heterogeneity of the enzyme caused by its oligomerization, *Biochemistry-Us 44*, 13902-13913.
32. Davydov, D. R., Sineva, E. V., Sistla, S., Davydova, N. Y., Frank, D. J., Sligar, S. G., and Halpert, J. R. (2010) Electron transfer in the complex of membrane-bound human cytochrome P450 3A4 with the flavin domain of P450BM-3: The effect of oligomerization of the heme protein and intermittent modulation of the spin equilibrium, *Bba-Bioenergetics 1797*, 378-390.
33. Denisov, I. G., Baas, B. J., Grinkova, Y. V., and Sligar, S. G. (2007) Cooperativity in cytochrome P450 3A4 - Linkages in substrate binding, spin state, uncoupling, and product formation, *J Biol Chem 282*, 7066-7076.

CHAPTER 4

In vitro Metabolic Stability Measurements without Chromatography or Mass Spectrometry

4.1 Abstract

In vitro metabolic stability measurements are a critical component of pre-clinical drug development. Available measurement strategies rely on chromatography and mass spectrometry, which are expensive, labor-intensive, and low-throughput. Using a reaction engineering approach, we have developed a general method to measure metabolic stability by fluorescently quantifying cofactors in the mechanisms of cytochrome P450 enzymes. This method combines the accuracy and generality of chromatography with the ease and throughput of fluorescence.

4.2 Introduction

Cytochrome P450 mediated oxidation is the primary route of first-pass drug metabolism in humans, and accounts for the metabolism of the majority of currently prescribed drugs (*1*). P450 enzymes use dissolved dioxygen and electrons from NADPH, supplied via a coenzyme reductase, to generate a highly reactive ferryl-oxo species (*2*). This reactive intermediate is used to oxidize a wide variety of exogenous drug compounds. Because these enzymes metabolize so many different compounds, there is a large risk for drug-drug interactions, where the presence of one drug inhibits the metabolism of another. If the drugs have a narrow therapeutic range, *in vivo* concentrations can reach toxic levels (*3*). As a result, determining which P450 enzymes react with a drug in development and the rate of this reaction is a critical part of pre-clinical testing (*4*).

Currently, the favored approach to measuring the rate of P450 oxidation of a compound, known as its metabolic stability, is with liquid chromatography coupled mass spectrometry (LCMS/MS) (*5*). This is necessary to successfully quantify a diverse array of compounds within the heterogeneous liver cell extracts that most accurately mimic *in vivo* drug metabolism. Although recent advances in high-throughput chromatographic systems coupled with liquids handling robots have drastically increased the potential throughput of LCMS/MS (*6*), this approach is limited by the equipment expense, difficulty of assay development, and the inherent sequential nature of chromatographic measurements. In contrast, fluorescence measurements can be taken in parallel, use cheaper equipment, are non-destructive such that time-course data rather than endpoints can be acquired, and are also ideally suited to isolate an analyte of interest within a heterogeneous system.

Several fluorogenic substrates have been developed to identify potential P450 interactions by measuring whether a test compound inhibits P450-mediated fluorophore generation (*7*). Although this method is very high-throughput, due to the complexity of the P450-substrate binding interaction, the inhibition data from these substrates do not generally correlate with data from traditional substrates (*8*). As a result, inhibition measurements with fluorogenic substrates are often a first test applied to the large number of compounds entering pre-clinical testing. As compounds are removed from consideration, more accurate and more expensive testing strategies can be applied,

culminating in the measurement of metabolic stability with LCMS/MS (*1*). Clearly, a method allowing metabolic stability data to be taken earlier on more compounds would greatly improve efficiency in the difficult process of drug development

To address this problem, we have developed the Metabolizing Enzyme Stability Assay Plate (MesaPlate), a simple and general approach to quantifying metabolic stability using fluorescence intensity measurements to calculate the concentration of species in the P450 reaction mechanism. These concentration measurements are then used to solve the overall rate equation for the depletion of substrate. Due to the large number of side products generated, it is impractical to measure all of the species that appear in the overall P450 rate equation (Fig 4.1A). We, instead, took a reaction engineering approach to simplify the rate equation with the addition of superoxide dismutase and catalase. These antioxidant enzymes act together to convert two of the side products, superoxide and hydrogen peroxide, into the third side product, water, without using additional reducing equivalents. This leaves only two effective reaction pathways in the overall system: substrate oxidation (Fig 4.1, Reaction 1) and water generation (Fig 4.1, Reaction 4). Thus, the rate of substrate oxidation ($-r_{RH}$), or metabolic stability, can be calculated from the rates of depletion of NADPH ($-r_{NADPH}$) and oxygen ($-r_{O2}$), each of which can be quantified with fluorescence intensity measurements using standard techniques (*9-11*). The derivation of these rate equations is shown in Appendix 4.1.

a

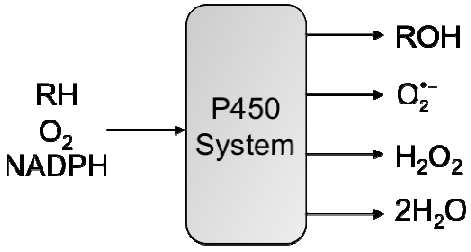

$$RH + O_2 + NADPH + H^+ \rightarrow ROH + NADP^+ + H_2O \quad (1)$$

$$O_2 + \tfrac{1}{2}NADPH \rightarrow O_2^{\bullet-} + \tfrac{1}{2}NADP^- - \tfrac{1}{2}H^+ \quad (2)$$

$$O_2 + NADPH + H^+ \rightarrow H_2O_2 + NADP^+ \quad (3)$$

$$O_2 + 2NADPH + 2H^+ \rightarrow 2H_2O + NADP^+ \quad (4)$$

$$(-r_{RH}) = 2(-r_{O_2}) - (-r_{NADPH}) - (r_{H_2O_2}) - (r_{O_2^{\bullet-}})$$

b

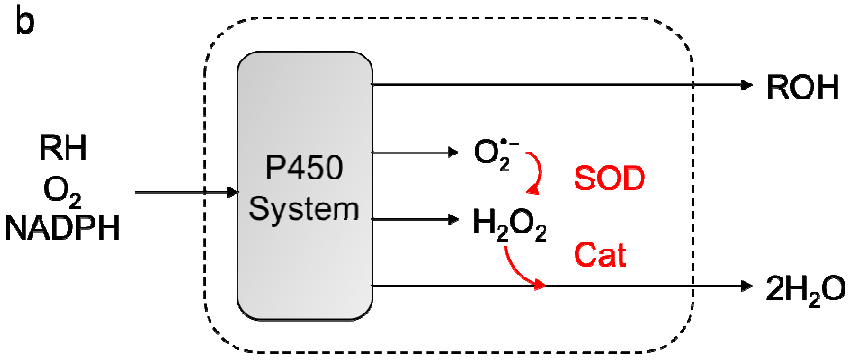

$$RH + O_2 + NADPH + H^+ \rightarrow ROH + NADP^+ + H_2O \quad (1)$$

$$O_2 + 2NADPH + 2H^+ \rightarrow 2H_2O + NADP^+ \quad (4)$$

$$(-r_{RH}) = 2(-r_{O_2}) - (-r_{NADPH})$$

Figure 4.1. Schematic of the P450 system, relevant reactions, and overall rate equation for metabolic stability, ($-r_{RH}$), before (a) and after (b) the addition of the antioxidant enzymes superoxide dismutase and catalase.

4.3 Materials and Methods

4.3.1 Materials

The substrates, testosterone, dextromethorphan, amitriptyline, racemic metoprolol, diclofenac, tolbutamide, 3-methylindole, and lidocaine; the inhibitors, 1-aminobenzotriazole and 1-phenylimidazole; the enzymes, catalase from bovine liver and superoxide dismutase from bovine erythrocytes; and nicotinamide adenine dinucleotide phosphate (NADPH) were purchased from Sigma (St. Louis, MO). PeroxyGreen1 (PG1) was a kind gift of Professor Chris Chang. Microsomes from baculovirus-infected insect cells (Baculosomes) expressing human P450 isoforms and rabbit cytochrome P450 reductase were purchased from Invitrogen (Carlsbad, Ca). Pooled human liver microsomes (catalog number 452161) were purchased from BD Biosciences (Woburn, MA). All chemicals were used as received.

4.3.2 Metabolic Stability Assay

Metabolic stability assays were prepared in triplicate for each condition tested. CYP3A4 containing Baculosomes was assayed at 25 nM, while all other P450 enzymes were assayed at 50 nM. CYP2C9 was assayed in 50 mM potassium phosphate, while all other P450 enzymes were assayed in 100 mM potassium phosphate. Test compounds for CYP2C9 were dissolved in DMSO and added to a final DMSO concentration of 0.5 %, while the test compounds for all other enzymes were dissolved in methanol and added to a final methanol concentration of 1%. CYP1A2 was assayed at pH 8.0, while all other assays were at pH 7.4. Experiments with pooled human liver microsomes were conducted at pH 7.4 in 100 mM potassium phosphate and a final methanol concentration of 1%. Catalase and superoxide dismutase were included in all assays at 100 U/mL and 50 U/mL, respectively. The MitoXpress oxygen probe (Luxcell Biosciences, Cork, Ireland) was reconstituted in deionized water and added to the reactions at a 15-fold dilution per the manufacturer's instructions. NADPH solutions were prepared fresh daily and the concentration was checked via absorbance using a molar extinction coefficient of 6.22 $mM^{-1}cm^{-1}$. Reactions were incubated for 20 min at room temperature before initiation with NADPH to a final concentration of 350 μM and a final volume of 100 μL in a 96-well plate. Directly after reaction initiation, samples were transferred to a 384-well quartz plate (JNETDirect Biosciences, Herndon, VA) and sealed with aluminum sealing film (Nunc, Rochester NY) such that no air bubbles were trapped in the wells. The reactions were followed via fluorescence intensity measurements in a Spectramax M5 plate reader (Molecular Devices, Sunnyvale CA) at 25 °C. Fluorescence intensity was simultaneously recorded at two excitation/emission wavelengths: 385 nm/460 nm for NADPH and 380 nm/650 nm for the oxygen probe.

MitoXpress is a fluorescent, platinum porphyrin that is collisionally quenched by dissolved oxygen. The relationship between probe fluorescence and oxygen concentration follows the well known Stern-Volmer expression as shown in Equation 5, where I_0 is the fluorescence intensity in the absence of quencher and I is the measured intensity (*12*).

$$\frac{I_0}{I} = 1 + K_{SV}[O_2] \qquad (5)$$

The Stern-Volmer quenching constant, K_{SV}, was calculated from a two-point oxygen calibration curve consisting of an air-saturated and a deoxygenated standard. The air saturated point was taken as the average of the initial oxygen signal from the assay wells while the deoxygenated standard was generated enzymatically with 50 nM CYP3A4, 100 μM testosterone, and 350 μM NADPH. Although the maximum absorbance of NADPH is at 340 nm, fluorescence excitation at 380 nm was chosen to reduce the inner-filter effect and increase standard curve linearity. NADPH standard curves fit well to a second order polynomial ($R^2 > 0.99$). On-plate standards for both oxygen and NADPH were included in each experiment and exhibited good day to day reproducibility (within 10%).

4.3.3 Chromatography

Chromatographic validation assays were conducted in duplicate at identical compositions as the multiwell plate assays, except without the addition of the oxygen probe. The CYP1A2 mediated depletion of lidocaine and 3-methylindole was quantified with gas chromatography. Reactions were stopped at 5 time points with the addition of an equal volume of hexane including internal standard. The organic phase was injected into a 25 m, 250 μm (ID) Varian FactorFour VF-5ms capillary column installed in a Varian 3900 gas chromatograph with an FID detector (Walnut Creek, CA). The injector and detector temperatures were 250 and 280 °C, respectively. The samples were injected at a split ratio of 20, with helium as the carrier gas at a flowrate of 2.0 mL/min. The column temperature was maintained at 60 °C for 2 min, ramped to 120 °C at a rate of 10 °C/min, and finally ramped to 250 °C at a rate of 45 °C/min, which was held for 5 min. The CYP2D6 mediated depletion of amitriptyline and metoprolol was quantified with high performance liquid chromatography (HPLC). Reactions were quenched at 4 time points with 100 uL of ice-cold methanol containing internal standard. Samples were analyzed on a 1200 series Agilent HPLC with a reverse-phase Alltech Prevail C18 3 μm 3.0x150 mm column with a 0.4 ml/min flow rate and a gradient of 40 – 90% methanol over 13 min with a constant 0.05% concentration of formic acid.

4.3.4 *In Situ* H_2O_2 measurement

The H_2O_2 probe, PG1, reacts in a 1:1 stoichiometry with H_2O_2 to produce the highly fluorescent Tokyo Green fluorophore (*13*). The reaction rate is first order in PG1 and in H_2O_2, which yields the rate law shown in Equation 6; however, since the reaction is slow on the time scale of the experiment, the concentration of PG changes little over the experiment. This allows the rate law to be simplified, as shown in Equation 9, such that the rate of change of TG is directly proportional to the concentration of H_2O_2. The rate law can be further simplified because the change in concentration of TG is directly proportional to the change in fluorescence in relative fluorescence units (RFU) as shown in Equation 7. Using Equation 7, k_D" was calculated to be 13.6 ± 0.1 RFU* μM^{-1}.

$$\frac{d[TG]}{dt} = k_D[PG][H_2O_2] \approx k_D'[H_2O_2] \quad (6)$$

$$\frac{d[TG]}{dt} = k_D[PG][H_2O_2] \approx \frac{d[RFU]}{dt} \approx k_D''[H_2O_2] \quad (7)$$

H_2O_2 was quantified by monitoring the increase in fluorescence signal at an excitation and emission wavelength of 490 nm and 520 nm of 5 μM PG1 in a CYP3A4 metabolic stability assays conducted as described above.

4.4. Results

Proof of concept experiments were conducted with Baculosomes, a model P450 system consisting of microsomes isolated from insect cells expressing a single P450 isoform with P450 reductase. Representative NADPH and oxygen depletion data for the CYP3A4 oxidation of testosterone are shown in Figure 4.2. Metabolic stability data for several P450 isoforms are shown in Figures 4.3 – 4.6 as a function of substrate concentration. The measured rates of NADPH and oxygen depletion are shown in Appendix 4.2. Except for the oxidation of amitriptyline by CYP2D6, which is known to display substrate inhibition (*14*), all data sets fit well to the Michaelis-Menten equation as shown with Eadie-Hofstee plots in Figure 4.3 – 4.6. In addition, the calculated catalytic constants and measured rates compare favorably with traditional chromatographic approaches (Table 4.1 - 4.2). Because the MesaPlate measures the total rate of P450 mediated oxidations, literature comparisons to substrates with multiple products (testosterone and dextromethorphan) are based on the calculated total rate of substrate depletion as described in Appendix 4.3.

To demonstrate the measurement of P450 inhibition, the inhibition of the CYP3A4 metabolism of testosterone by two types of inhibitors is shown in Figure 4.7. An example of reversible inhibition is seen with 1-phenylimidazole (PIM) (Fig. 4.7A), which reversibly binds to the iron center of the heme cofactor (*15*). Irreversible inhibition is seen with 1-aminobenzotriazole (ABT) (Fig. 4.7B), which is activated via P450 oxidation to alkylate the heme cofactor and prevent further catalysis (*16*). Interestingly, the rate measured at high ABT concentrations appears to level off at 3.7 ± 1.1 nmol/min/nmol P450, which may represent the catalysis necessary to activate this inhibitor. The calculated IC_{50} values of 2.4 μM and 0.12 μM for PIM and ABT, respectively, compare well with literature values of 2.7 μM (*17*) and 0.58 μM (*18*).

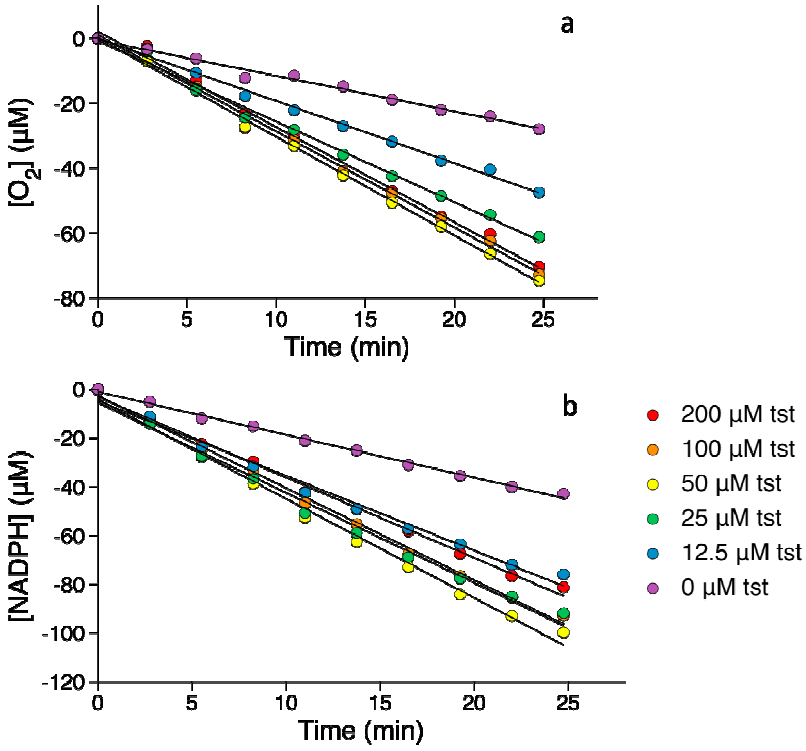

Figure 4.2. Rates of depletion of (a) NADPH and (b) oxygen in the CYP3A4 oxidation of testosterone.

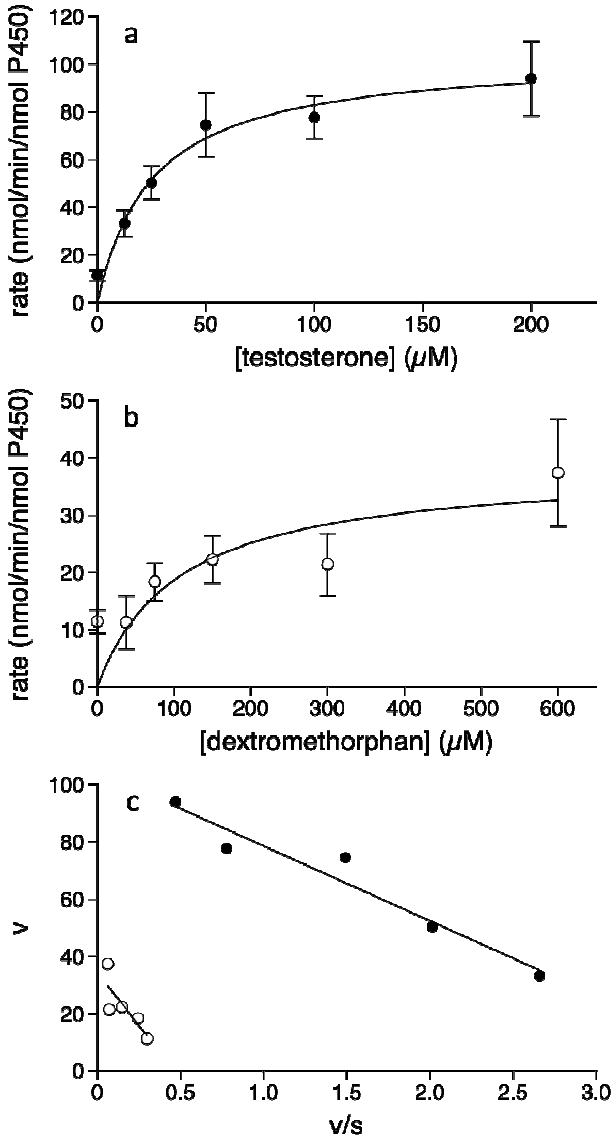

Figure 4.3. Measured rate of oxidation of (a) testosterone and (b) dextromethorphan by CYP3A4 and (c) an Eadie-Hofstee plot of these rates.

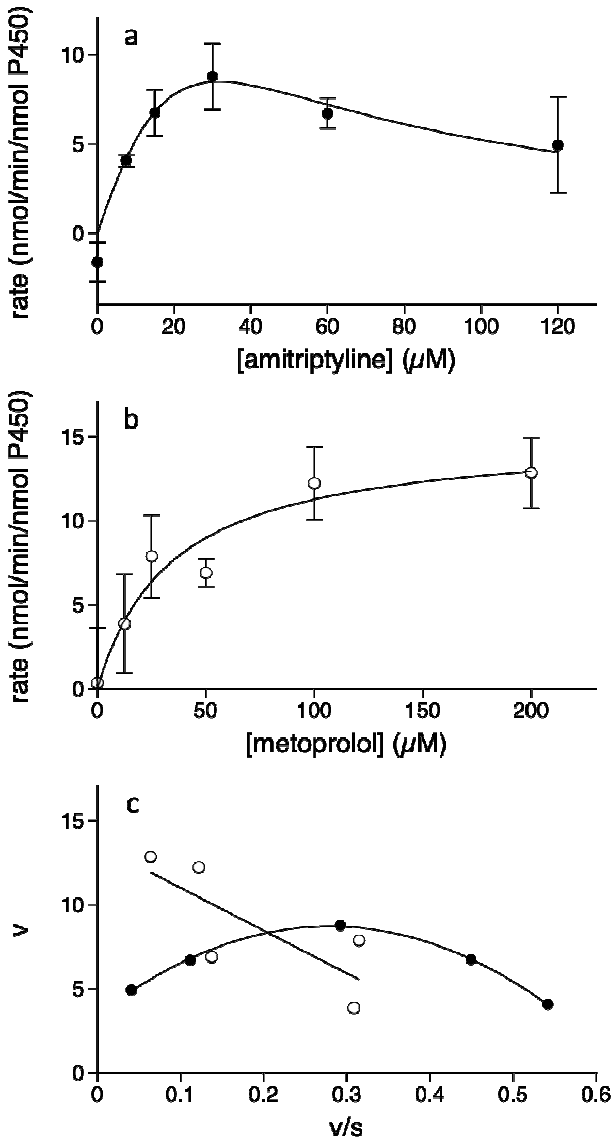

Figure 4.4. Measured rate of oxidation of (a) amitriptyline and (b) metoprolol by CYP2D6 and (c) an Eadie-Hofstee plot of these rates. Note that the metabolism of amitriptyline exhibits substrate inhibition.

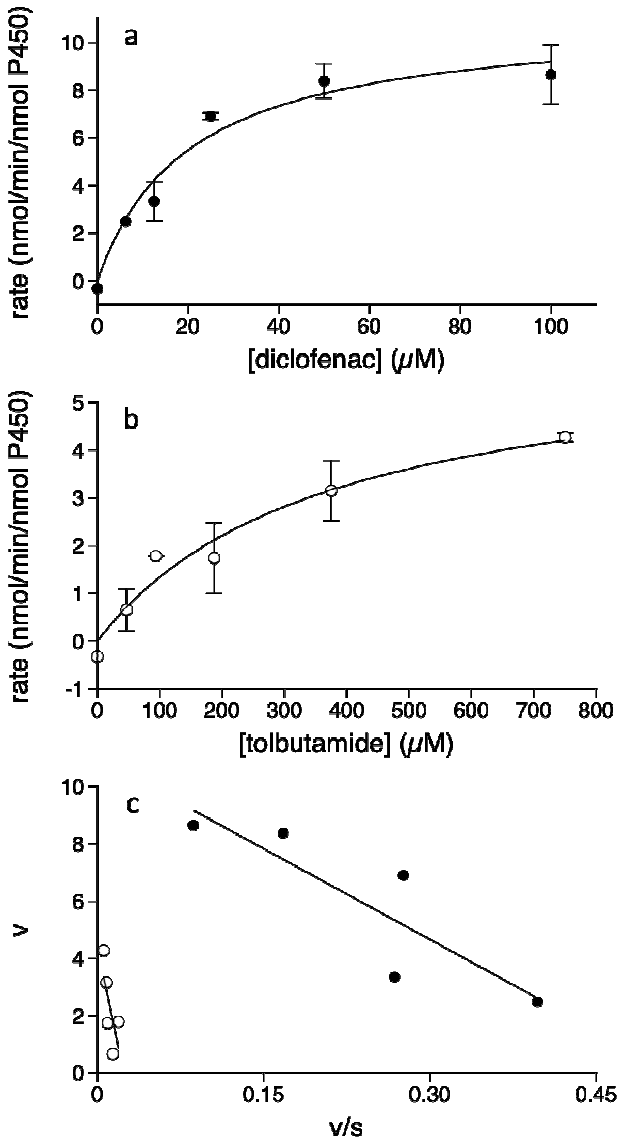

Figure 4.5. Measured rate of oxidation of (a) diclofenac and (b) tolbutamide by CYP2C9 and (c) an Eadie-Hofstee plot of these rates

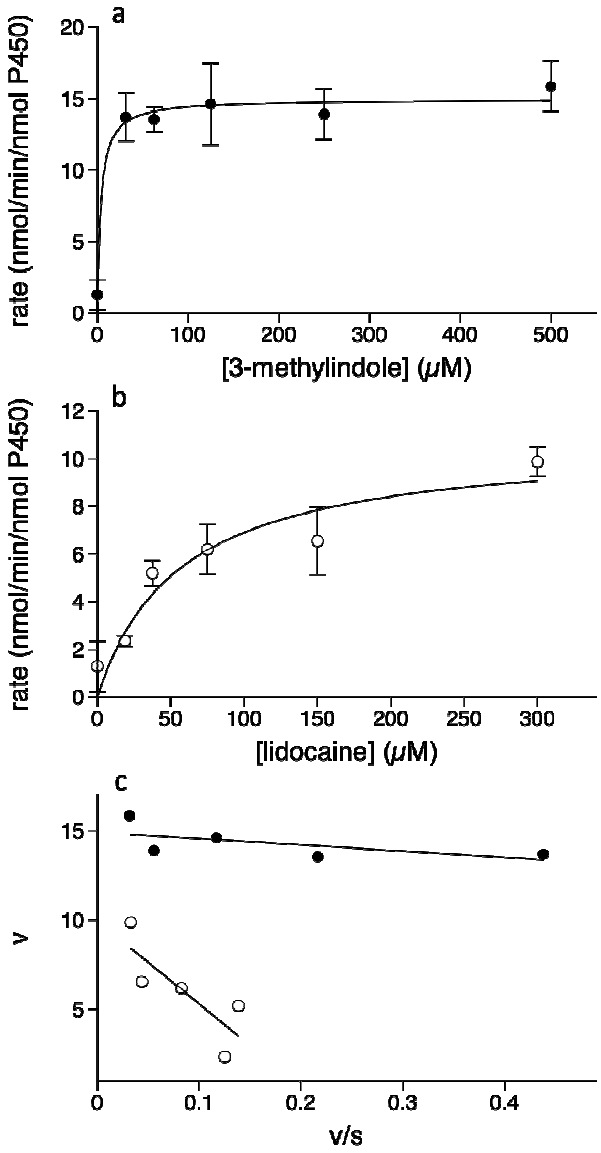

Figure 4.6. Measured rate of oxidation of (a) 3-methylindole and (b) lidocaine by CYP1A2 and (c) an Eadie-Hofstee plot of these rates.

		MesaPlate		Literature	
Enzyme	Substrate	kcat	Km	kcat	Km
CYP3A4	Testosterone	118.2 ± 8.0	31.4 ± 6.6	105.4	24.6
CYP3A4	Dextromethorphan	38.4 ± 7.8	105.8 ± 64.0	26.5	210.4
CYP2C9	Diclofenac	11.1 ± 1.3	20.2 ± 7.0	29	5.1
CYP2C9	Tolbutamide	6.3 ± 1.2	366.0 ± 153.6	10.1	103

Table 4.1. Comparison of the catalytic constants k_{cat} (nmol/min/nmol P450) and K_M (μM) from the MesaPlate to literature values (*19-21*). Catalytic constants for testosterone and dextromethorphan are calculated as described in Appendix 4.2.

		MesaPlate	Chromatography
Enzyme	Substrate	$-r_{RH}$	$-r_{RH}$
CYP2D6	Amitriptyline	6.7 ± 0.8	3.8 ± 0.4
CYP2D6	Metoprolol	12.2 ± 2.2	9.8 ± 2.3
CYP1A2	3-methylindole	15.8 ± 1.4	10.7 ± 0.8
CYP1A2	lidocaine	11.5 ± 2.1	9.7 ± 1.2

Table 4.2. Comparison of metabolic stabilities (nmol/min/nmol P450) measured with the MesaPlate and with chromatography.

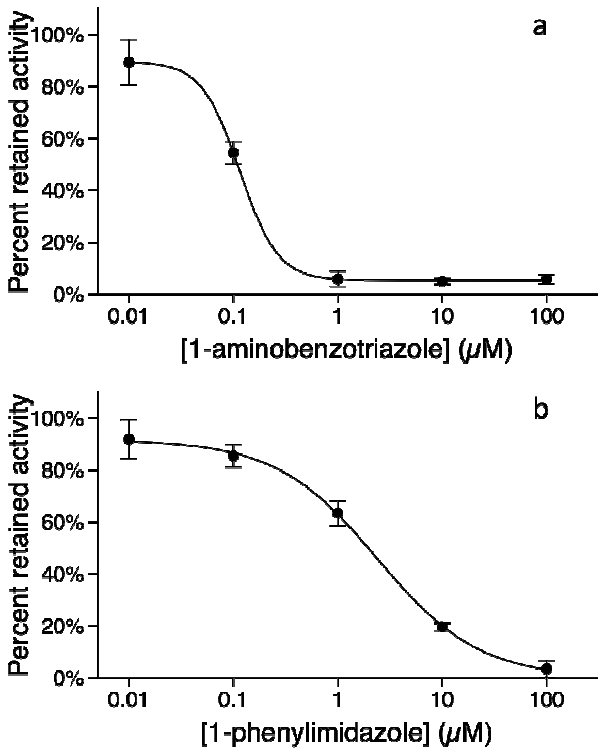

Figure 4.7. Inhibition of CYP3A4 testosterone metabolism by (a) 1-phenylimidazole and (b) 1-aminobenzotriazole. Data were fit to a four parameter logistic equation.

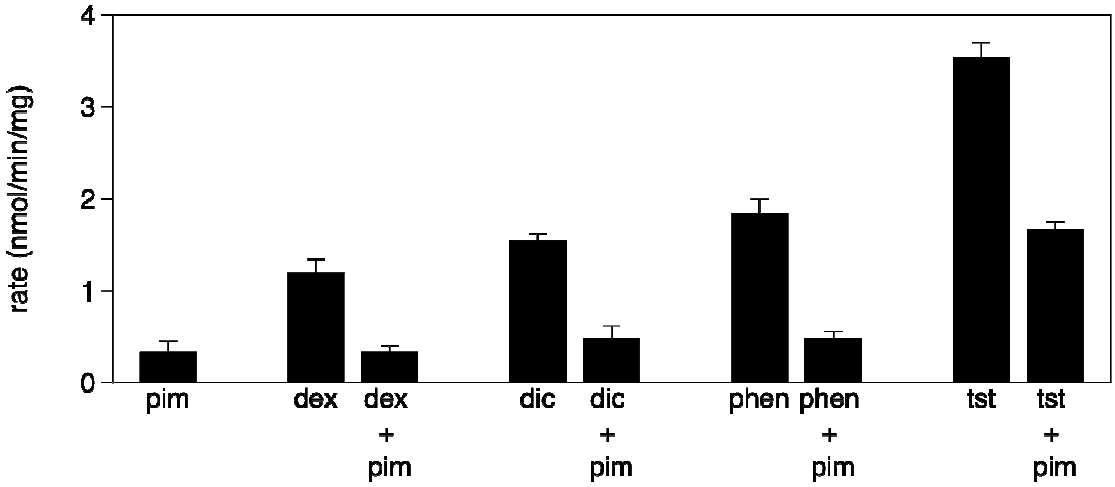

Figure 4.8. Demonstration of the measurement of metabolic stability in human liver microsomes showing the inhibition of CYP2D6 metabolism of dextromethorphan (dex), CYP2C9 metabolism of diclofenac (dic), CYP1A2 metabolism of phenacetin (phen), and CYP3A4 metabolism of testosterone (tst) by the inhibitor, 1-phenylimidazole (pim).

To demonstrate the MesaPlate with a more pharmaceutically relevant system, isoform specific substrates were incubated with pooled human liver microsomes in the presence or absence of PIM (Fig 4.8). A clear trend is observed where the measured rate of P450 oxidation is much lower in the presence of inhibitor.

The addition of SOD and catalase to the reaction medium insures that superoxide and hydrogen peroxide do not significantly accumulate. Thus, the overall rates of change of superoxide ($r_{O2\bullet-}$) and hydrogen peroxide (r_{H2O2}) are much smaller than the rates of change of the substrates ($-r_{NADPH}$, $-r_{O2}$, $-r_{RH}$). Because $r_{O2\bullet-}$ and r_{H2O2} are both negligible compared to $-r_{NADPH}$, $-r_{O2}$, and $-r_{RH}$, the overall rate equation is simplified to the final form shown in Figure 4.1B. The validity of this pseudo-steady state assumption (PSSA) can be verified via measurement and calculation. We measured the in situ concentration of H_2O_2 during the oxidation of testosterone by CYP3A4 with PG1, a fluorogenic peroxide probe. PG1 is a protected fluorescent molecule that is specifically deprotected by hydrogen peroxide, generating a fluorescent signal (*13*). The rate of deprotection, and thus of fluorescence signal increase, is directly proportional to the concentration of hydrogen peroxide (Fig. 4.9A). We found that the rate of increase of signal during the CYP3A4 oxidation of testosterone was effectively constant (Fig. 4.9B). This indicates that the concentration of H_2O_2 is also effectively constant. In addition, the calculated H_2O_2 concentrations were quite low, varying between 0.8 and 1.8 μM as a function of substrate concentration (Fig. 4.9C). Compared to the large rates of oxygen and NADPH depletion observed (Fig 4.2), r_{H2O2} is negligible, which validates the use of the PSSA. In general, though, SOD and catalase are both diffusion-limited enzymes, so the antioxidant abilities of SOD and catalase exceed the potential production of oxidants by the P450 and neither superoxide nor H_2O_2 are expected to accumulate.

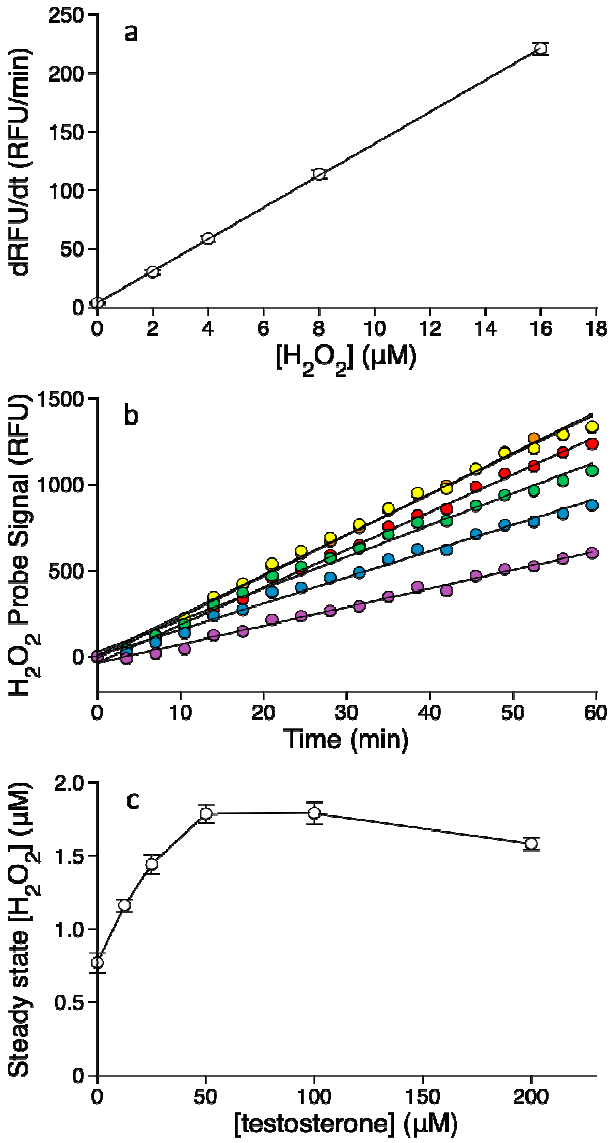

Figure 4.9. In situ hydrogen peroxide measurements were taken with the peroxide probe, PG1, which displays (a) first order kinetics yielding a linear relationship between the rate of increase of fluorescence in relative fluorescence units (RFU) to the concentration of hydrogen peroxide. A linear increase in probe signal (b) for 6 concentrations of testosterone (same color scheme as Fig 4.2) metabolized by CYP3A4 yields (c) low steady state hydrogen peroxide concentrations.

4.5 Discussion

The value of the MesaPlate can be demonstrated with a simple cost analysis of the MesaPlate versus a traditional LCMS/MS approach. This is shown in Table 4.3. The equipment costs shown are rough estimates from vendors, while the yearly operating cost is assumed to include a maintenance contract at 5% of the initial cost plus the total salary and benefits of one person for upkeep and maintenance of an LCMS/MS, which is assumed to be roughly $150 k. While these numbers are rough estimates, it is clear that the overall cost of the MesaPlate system is much less than that of an LCMS/MS. The time estimate for the MesaPlate is conservative based on using 300 wells of a 384 well plate, while the estimate for LCMS/MS comes from the literature (*6*). Again, although this is a rough estimate, the MesaPlate system is also much faster than LCMS/MS. This overall advantage will only grow with increases in throughput via automation and miniaturization of the physical system to higher density multiwell plates or microscale chip arrays.

	High-throughput LCMS/MS	MesaPlate
Instrument Cost	$400k	$50k
Yearly Maintenance	$170k	$2.5k
Time for 150 samples	(150 samples) x (4 time points) x (2 replicates) x (1 min/assay) = 20 hrs	(150 samples) x (2 replicates) x (3 hrs/plate) = 3 hrs

Table 4.3. Simplified cost and throughput comparison of the MesaPlate with traditional high-throughput LCMS/MS

In conclusion, we have developed a high-throughput approach to metabolic stability measurements. This technology, based on fluorescently acquired data, represents a new approach to metabolic stability measurements and promises to decrease the cost of drug development and offer higher quality decision-making information earlier in the drug development process.

4.6 References

1. Wienkers, L. C., and Heath, T. G. (2005) Predicting in vivo drug interactions from in vitro drug discovery data, *Nature Reviews Drug Discovery 4*, 825-833.
2. Denisov, I. G., Makris, T. M., Sligar, S. G., and Schlichting, I. (2005) Structure and chemistry of cytochrome P450, *Chem Rev 105*, 2253-2277.
3. Lazarou, J., Pomeranz, B. H., and Corey, P. N. (1998) Incidence of adverse drug reactions in hospitalized patients - A meta-analysis of prospective studies, *Jama-J Am Med Assoc 279*, 1200-1205.
4. Bjornsson, T. D., Callaghan, J. T., Einolf, H. J., Fischer, V., Gan, L., Grimm, S., Kao, J., King, S. P., Miwa, G., Ni, L., Kumar, G., McLeod, J., Obach, R. S., Roberts, S., Roe, A., Shah, A., Snikeris, F., Sullivan, J. T., Tweedie, D., Vega, J. M., Walsh, J., and Wrighton, S. A. (2003) The conduct of in vitro and in vivo drug-drug interaction studies: A Pharmaceutical Research and Manufacturers of America (PhRMA) perspective, *Drug Metab Dispos 31*, 815-832.

5. Youdim, K. A., and Saunders, K. C. (2010) A review of LC-MS techniques and high-throughput approaches used to investigate drug metabolism by cytochrome P450s, *J Chromatogr B 878*, 1326-1336.
6. Xu, R. D., Manuel, M., Cramlett, J., and Kassel, D. B. (2010) A high throughput metabolic stability screening workflow with automated assessment of data quality in pharmaceutical industry, *J Chromatogr A 1217*, 1616-1625.
7. Stresser, D. M., Turner, S. D., Blanchard, A. P., Miller, V. P., and Crespi, C. L. (2002) Cytochrome P450 fluorometric substrates: identification of isoform-selective probes for rat CYP2D2 and human CYP3A4, *Drug Metab Dispos 30*, 845-852.
8. Cohen, L. H., Remley, M. J., Raunig, D., and Vaz, A. D. N. (2003) In vitro drug interactions of cytochrome P450: An evaluation of fluorogenic to conventional substrates, *Drug Metab Dispos 31*, 1005-1015.
9. Lakowicz, J. R. (2006) *Principles of fluorescence spectroscopy*, 3rd ed., Springer, New York.
10. O'donovan, C., Hynes, J., Yashunski, D., and Papkovsky, D. B. (2005) Phosphorescent oxygen-sensitive materials for biological applications, *Journal of Materials Chemistry 15*, 2946-2951.
11. Papkovsky, D. B. (2004) Methods in optical oxygen sensing: Protocols and critical analyses, *Oxygen Sensing 381*, 715-735.
12. Will, Y., Hynes, J., Ogurtsov, V. I., and Papkovsky, D. B. (2006) Analysis of mitochondrial function using phosphorescent oxygen-sensitive probes, *Nat Protoc 1*, 2563-2572.
13. Miller, E. W., Tulyanthan, O., Isacoff, E. Y., and Chang, C. J. (2007) Molecular imaging of hydrogen peroxide produced for cell signaling, *Nature Chemical Biology 3*, 263-267.
14. Venkatakrishnan, K., Greenblatt, D. J., von Moltke, L. L., Schmider, J., Harmatz, J. S., and Shader, R. I. (1998) Five distinct human cytochromes mediate amitriptyline N-demethylation in vitro: Dominance of CYP 2C19 and 3A4, *J Clin Pharmacol 38*, 112-121.
15. Poulos, T. L., and Howard, A. J. (1987) Crystal-Structures of Metyrapone-Inhibited and Phenylimidazole-Inhibited Complexes of Cytochrome-P-450cam, *Biochemistry-Us 26*, 8165-8174.
16. Demontellano, P. R. O., and Mathews, J. M. (1981) Autocatalytic Alkylation of the Cytochrome-P-450 Prosthetic Heme Group by 1-Aminobenzotriazole - Isolation of an Nn-Bridged Benzene-Protoporphyrin Ix Adduct, *Biochem J 195*, 761-764.
17. Fowler, S. M., Riley, R. J., Pritchard, M. P., Sutcliffe, M. J., Friedberg, T., and Wolf, C. R. (2000) Amino acid 305 determines catalytic center accessibility in CYP3A4, *Biochemistry-Us 39*, 4406-4414.
18. Emoto, C., Murase, S., Sawada, Y., and Iwasaki, K. (2005) In vitro inhibitory effect of 1-aminobenzotriazole on drug oxidations in human liver microsomes: a comparison with SKF-525A, *Drug Metab Pharmacokinet 20*, 351-357.
19. Krauser, J. A., and Guengerich, F. P. (2005) Cytochrome P450 3A4-catalyzed testosterone 6 beta-hydroxylation stereochemistry, kinetic deuterium isotope effects, and rate-limiting steps, *J Biol Chem 280*, 19496-19506.

20. Kumar, V., Rock, D. A., Warren, C. J., Tracy, T. S., and Wahlstrom, J. L. (2006) Enzyme source effects on CYP2C9 kinetics and inhibition, *Drug Metab Dispos 34*, 1903-1908.
21. Yu, A. M., and Haining, R. L. (2001) Comparative contribution to dextromethorphan metabolism by cytochrome P450 isoforms in vitro: Can dextromethorphan be used as a dual probe for both CYP2D6 and CYP3A activities?, *Drug Metab Dispos 29*, 1514-1520.

Appendix 4.1 Kinetic Analyses of the P450 Reaction System

Appendix 4.1.1 Kinetic analysis of the P450 system

$$RH + O_2 + NADPH + H^+ \rightarrow ROH + NADP^+ + H_2O \quad (1)$$

$$O_2 + NADPH + H^+ \rightarrow H_2O_2 + NADP^+ \quad (2)$$

$$O_2 + 2NADPH + 2H^+ \rightarrow 2H_2O + NADP^+ \quad (3)$$

$$O_2 + \frac{1}{2}NADPH \rightarrow O_2^{\bullet -} + \frac{1}{2}NADP^+ + \frac{1}{2}H^+ \quad (4)$$

Overall Reaction Rates

Reaction 1: $-r_{1RH} = -r_{1O_2} = -r_{1NADPH} = r_{1ROH}$

Reaction 2: $-r_{2O_2} = -r_{2NADPH} = r_{2H_2O_2}$

Reaction 3: $-r_{3O_2} = -\frac{1}{2}r_{3NADPH}$

Reaction 4: $-r_{4O_2} = -2r_{4NADPH} = r_{4O_2^{\bullet -}}$

Net Rates

$r_{O_2} = r_{1O_2} + r_{2O_2} + r_{3O_2} + r_{4O_2}$

$r_{NADPH} = r_{1NADPH} + r_{2NADPH} + r_{3NADPH} + r_{4NADPH}$

$r_{H_2O_2} = r_{2H_2O_2}$

$r_{O_2^{\bullet -}} = r_{4O_2^{\bullet -}}$

From Net Rates

$-r_{3O_2} = -r_{O_2} + r_{1O_2} + r_{2O_2} + r_{4O_2}$

$-\frac{1}{2}r_{3NADPH} = -\frac{1}{2}r_{NADPH} + \frac{1}{2}r_{1NADPH} + \frac{1}{2}r_{2NADPH} + \frac{1}{2}r_{4NADPH}$

Equating the two

$$-r_{O_2} + r_{1O_2} + r_{2O_2} + r_{4O_2} = -\frac{1}{2}r_{NADPH} + \frac{1}{2}r_{1NADPH} + \frac{1}{2}r_{2NADPH} + \frac{1}{2}r_{4NADPH}$$

Where

$r_{1O_2} = r_{1RH} = r_{1NADPH}$

$r_{2O_2} = r_{2NADPH} = -r_{2H_2O_2} = -r_{H_2O_2}$

$r_{4O_2} = -r_{4O_2^{\bullet -}} = -r_{O_2^{\bullet -}} + r_{5O_2^{\bullet -}} = -r_{O_2^{\bullet -}}$

$r_{4NADPH} = -\frac{1}{2}r_{4O_2^{\bullet -}} = -\frac{1}{2}r_{O_2^{\bullet -}}$

Thus

$$-r_{O_2} + r_{RH} - r_{H_2O_2} - r_{O_2^{\bullet-}} = -\frac{1}{2}r_{NADPH} + \frac{1}{2}r_{RH} - r_{H_2O_2} - \frac{1}{2}r_{O_2^{\bullet-}}$$

Solve for $-r_{RH}$, where each value in parenthesis is a positive quantity

$$(-r_{RH}) = 2(-r_{O_2}) - (-r_{NADPH}) - (r_{H_2O_2}) - (r_{O_2^{\bullet-}})$$

Appendix 4.1.2. Kinetic analysis of the P450 system with the Addition of Superoxide Dismutase and Catalase

$$RH + O_2 + NADPH + H^+ \rightarrow ROH + NADP^+ + H_2O \quad (1)$$

$$O_2 + NADPH + H^+ \rightarrow H_2O_2 + NADP^+ \quad (2)$$

$$O_2 + 2NADPH + 2H^+ \rightarrow 2H_2O + NADP^+ \quad (3)$$

$$O_2 + \frac{1}{2}NADPH \rightarrow O_2^{\bullet-} + \frac{1}{2}NADP^+ + \frac{1}{2}H^+ \quad (4)$$

$$2O_2^{\bullet-} + 2H^+ \rightarrow O_2 + H_2O_2 \quad (5)$$

$$2H_2O_2 \rightarrow O_2 + 2H_2O \quad (6)$$

Overall Reaction Rates

$$\text{Reaction 1}: -r_{1RH} = -r_{1O_2} = -r_{1NADPH} = r_{1ROH}$$

$$\text{Reaction 2}: -r_{2O_2} = -r_{2NADPH} = r_{2H_2O_2}$$

$$\text{Reaction 3}: -r_{3O_2} = -\frac{1}{2}r_{3NADPH}$$

$$\text{Reaction 4}: -r_{4O_2} = -2r_{4NADPH} = r_{4O_2^{\bullet-}}$$

$$\text{Reaction 5}: -\frac{1}{2}r_{5O_2^{\bullet-}} = r_{5O_2} = r_{5H_2O_2}$$

$$\text{Reaction 6}: -\frac{1}{2}r_{6H_2O_2} = r_{6O_2}$$

Net Rates

$$r_{O_2} = r_{1O_2} + r_{2O_2} + r_{3O_2} + r_{4O_2} + r_{5O_2} + r_{6O_2}$$

$$r_{NADPH} = r_{1NADPH} + r_{2NADPH} + r_{3NADPH} + r_{4NADPH}$$

$$r_{H_2O_2} = r_{2H_2O_2} + r_{5H_2O_2} + r_{6H_2O_2}$$

$$r_{O_2^{\bullet-}} = r_{4O_2^{\bullet-}} + r_{5O_2^{\bullet-}}$$

From Net Rates

$$- r_{3O_2} = -r_{O_2} + r_{1O_2} + r_{2O_2} + r_{4O_2} + r_{5O_2} + r_{6O_2}$$

$$- \frac{1}{2} r_{3NADPH} = - \frac{1}{2} r_{NADPH} + \frac{1}{2} r_{1NADPH} + \frac{1}{2} r_{2NADPH} + \frac{1}{2} r_{4NADPH}$$

Equating the two

$$- r_{O_2} + r_{1O_2} + r_{2O_2} + r_{4O_2} + r_{5O_2} + r_{6O_2} = - \frac{1}{2} r_{NADPH} + \frac{1}{2} r_{1NADPH} + \frac{1}{2} r_{2NADPH} + \frac{1}{2} r_{4NADPH}$$

Where

$$r_{1O_2} = r_{1RH} = r_{1NADPH}$$

$$r_{2O_2} = r_{2NADPH} = -r_{2H_2O_2} = -r_{H_2O_2} + r_{5H_2O_2} + r_{6H_2O_2}$$

$$r_{4O_2} = -r_{4O_2^{\bullet -}} = -r_{O_2^{\bullet -}} + r_{5O_2^{\bullet -}} = -r_{O_2^{\bullet -}} - 2r_{5H_2O_2}$$

$$r_{5O_2} = r_{5H_2O_2}$$

$$r_{6O_2} = - \frac{1}{2} r_{6H_2O_2}$$

$$r_{4NADPH} = - \frac{1}{2} r_{4O_2^{\bullet -}} = - \frac{1}{2} r_{O_2^{\bullet -}} - r_{5H_2O_2}$$

Thus

$$- r_{O_2} + r_{RH} + \left[- r_{H_2O_2} + r_{5H_2O_2} + r_{6H_2O_2} \right] + \left[- r_{O_2^{\bullet -}} - 2r_{5H_2O_2} \right] + r_{5H_2O_2} - \frac{1}{2} r_{6H_2O_2} =$$

$$- \frac{1}{2} r_{NADPH} + \frac{1}{2} r_{RH} + \frac{1}{2} \left[- r_{H_2O_2} + r_{5H_2O_2} + r_{6H_2O_2} \right] + \frac{1}{2} \left[- \frac{1}{2} r_{O_2^{\bullet -}} - r_{5H_2O_2} \right]$$

Solve for $- r_{RH}$, where each value in parenthesis is a positive quantity

$$\left(- r_{RH} \right) = 2 \left(- r_{O_2} \right) - \left(- r_{NADPH} \right) - \left(r_{H_2O_2} \right) - \frac{2}{3} \left(r_{O_2^{\bullet -}} \right)$$

Pseudo - steady state assumption on H_2O_2 and $O_2^{\bullet -}$

$$\left(- r_{RH} \right) = 2 \left(- r_{O_2} \right) - \left(- r_{NADPH} \right)$$

Appendix 4.2 Measured NADPH and O_2 Depletion Rates

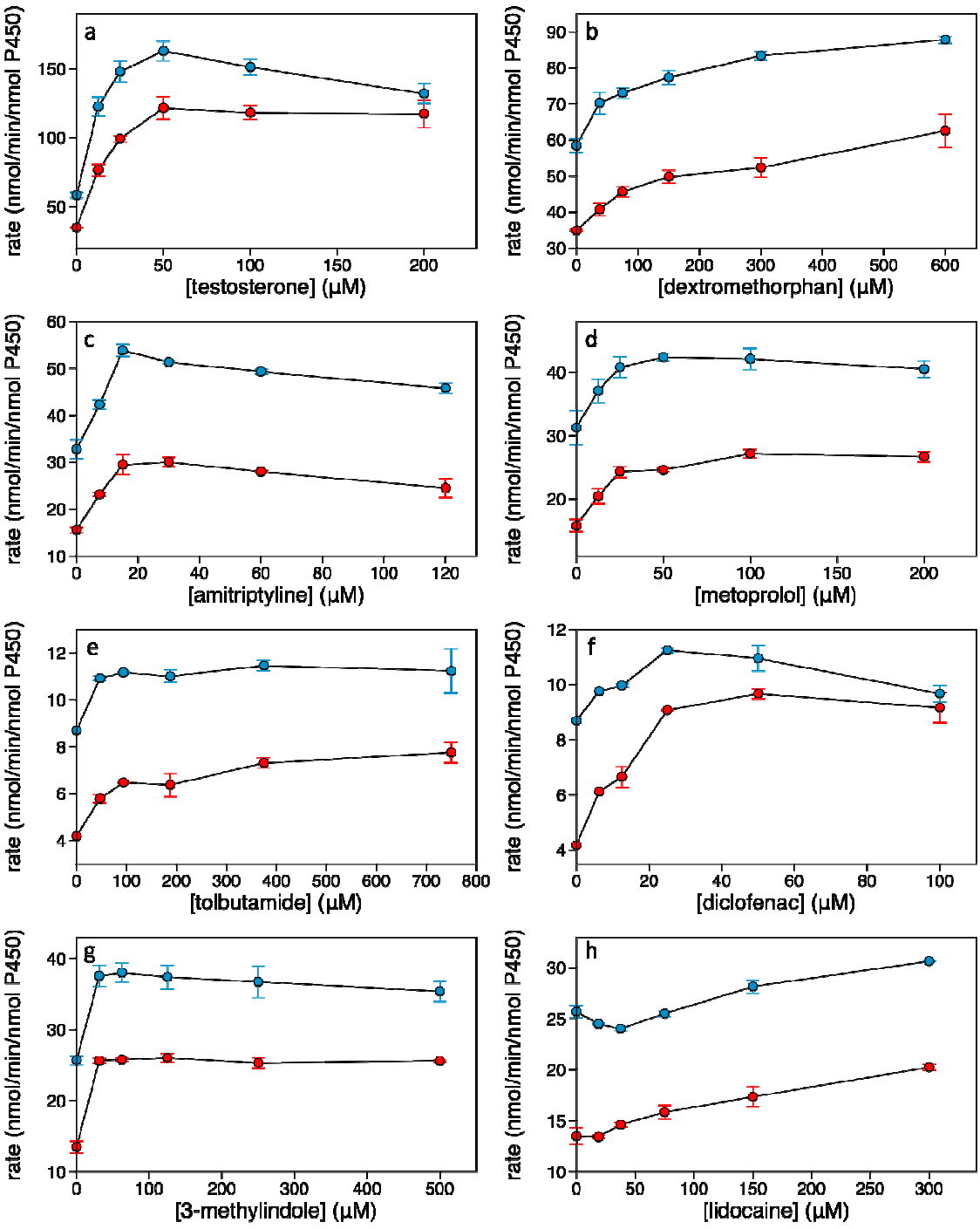

Figure 4.10. Measured rates of depletion of (blue circles) NADPH and (red circles) oxygen in the CYP3A4 oxidation of (a) testosterone and (b) dextromethorphan, the CYP2D6 oxidation of (c) amitriptyline and (d) metoprolol, the CYP2C9 oxidation of (e) diclofenac and (f) tolbutamide, and the CYP1A2 oxidation of (g) 3-methylindole and (h) lidocaine.

Appendix 4.3 Modeling Substrate Depletion when Multiple Products are Generated

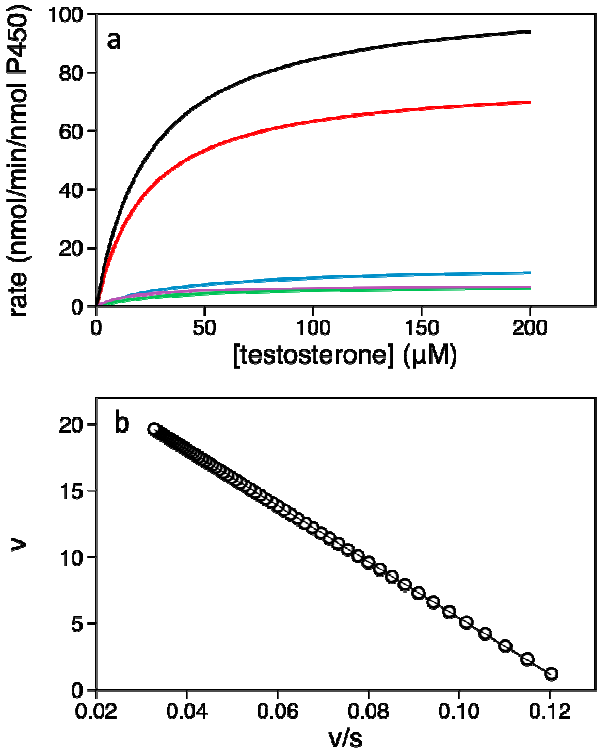

Figure 4.11. Modeling the rate of substrate depletion in the CYP3A4 oxidation of testosterone with (a) the black curve representing the sum of the rate of generation of the major product species, each of which is shown with a colored curve, and (b) the Eadie-Hofstee plot of testosterone depletion from which catalytic constants were extracted.

	6β-hydroxylation	2β-hydroxylation	15β-hydroxylation	1β-hydroxylation	Total
kcat	78	14	7.1	7.1	105.4
Km	23	44	32	17	24.6

Table 4.4. Literature values of the catalytic constants for the major products of the CYP3A4 oxidation of testosterone and the calculated catalytic constants for testosterone depletion.

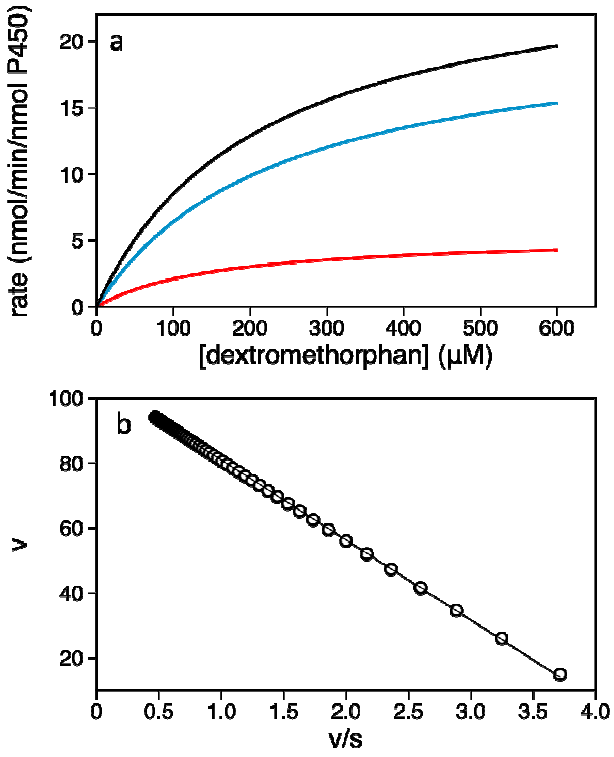

Figure 4.12. Modeling the rate of substrate depletion in the CYP3A4 oxidation of dextromethorphan with (a) the black curve representing the sum of the rate of generation of the major product species, each of which is shown with a colored curve, and (b) the Eadie-Hofstee plot of dextromethorphan depletion from which catalytic constants were extracted.

	O-demethylation	N-demethylation	Total
kcat	5.4	21.3	26.5
Km	157	232	210.4

Table 4.4. Literature values of the catalytic constants for the major products of the CYP3A4 oxidation of dextromethorphan and the calculated catalytic constants for dextromethorphan depletion.